BCL2 Regulates Differentiation of Intestinal Fibroblasts

Weder, Bruce ; Mamie, Céline ; Rogler, Gerhard ; Clarke, Stephen ; McRae, Bradford ; Ruiz, Pedro A ; Hausmann, Martin

Abstract: Background Fibrosis in patients with Crohn's disease (CD) results from an imbalance toward excessive fibrous tissue formation driven by fibroblasts. Activation of fibroblasts is linked to the B-cell lymphoma 2 (BCL2) family, which is involved in the induction of apoptosis. We investigated the impact of BCL2 repression on fibrogenesis. Methods The model of dextran sodium sulfate (DSS)-induced chronic colitis and the heterotopic transplantation model of fibrosis were used. Following the administration of the BCL2 antagonist (ABT-737, 50 mg/kg/d), collagen layer thickness and hydroxyproline (HYP) content were determined. Fibroblasts were stimulated with the BCL2 antagonist (0.01-100 µM). BCL2, alpha smooth muscle actin (SMA), and collagen I (COL1A1) were determined by quantitative polymerase chain reaction (qPCR), immunofluorescence microscopy (IF), and western blot (WB). mRNA expression pattern was determined by next-generation sequencing (NGS). Results Collagen layer thickness was significantly decreased in both DSS-induced chronic colitis and the transplantation model of fibrosis upon BCL2 antagonist administration compared with vehicle. Decreased HYP content confirmed the preventive effects of the BCL2 antagonist on fibrosis. In vitro, a significant increase in PI+/annexin V+ human colonic fibroblasts was determined by fluorescence-activated cell sorting upon treatment with high-dose BCL2 antagonist; at a lower dose, SMA, COL1A1, and TGF were decreased. NGS, IF, and qPCR revealed decreased expression and nuclear translocation of GATA6 and SOX9, known for reprogramming fibroblasts. Conclusion BCL2 antagonist administration partially prevented fibrogenesis in both fibrosis models. The BCL2 antagonist reduced the expression of TGF -induced factors involved in differentiation of myofibroblasts, and therefore might represent a potential treatment option against CD-associated fibrosis.

DOI: https://doi.org/10.1093/ibd/izy147

Accepted for publication at Inflammatory Bowel Diseases
Mar 08 2018 09:14AM

BCL2 regulates differentiation of intestinal fibroblasts

Bruce Weder MSc[1], Céline Mamie MSc [1], Gerhard Rogler MD PhD[1], Stephen Clarke PhD[2], Bradford McRae PhD[2], Pedro A. Ruiz PhD[1], Martin Hausmann PhD[1]

[1] Department of Gastroenterology and Hepatology, University Hospital Zurich, Zurich, Switzerland

[2] AbbVie Bioresearch Center, AbbVie Worcester, MA, USA

Short title: Differentiation of fibroblasts upon BCL2 antagonist treatment

List of how each author was involved with the manuscript:

- study concept: M Hausmann
- acquisition of data: B Weder
- critical revision of the manuscript: PA Ruiz, G Rogler, S Clarke, B McRae
- technical support: C Mamie

Disclosure: GR discloses grant support from AbbVie, Ardeypharm, MSD, FALK, Flamentera, Novartis, Roche, Tillots, UCB and Zeller. MH discloses grant support from AbbVie and Novartis. BW, CM, SC, BMR and PR have nothing to disclose.

Financial support: This research was supported by grant IBD-0324R from the Broad Medical Research Foundation (BMRF) to MH. This research was also supported by grant N°2013-16 from the Swiss inflammatory bowel disease cohort study (SIBDCS) to MH and by grant 314730_152895 from the Swiss National Science Foundation.

Address for correspondence:
Martin Hausmann PhD
Department of Gastroenterology and Hepatology
University Hospital Zürich
University of Zurich
Ramistrasse 100, 8091 Zurich
CH-Switzerland
Mail: martin.hausmann@usz.ch
Tel.: +41 44 255 9916
Fax.: +41 44 255 9496

Abstract

BACKGROUND: Fibrosis in patients with Crohn's disease (CD) results from an imbalance towards excessive fibrous tissue formation driven by fibroblasts. Activation of fibroblasts is linked to the B-cell lymphoma (BCL)2 family, which is involved in the induction of apoptosis. We investigated the impact of BCL2 repression on fibrogenesis.

METHODS: The model of dextran sodium sulfate (DSS)-induced chronic colitis, and the heterotopic transplantation model of fibrosis were used. Following the administration of the BCL2 antagonist (ABT-737, 50 mg/kg/day), collagen layer thickness and hydroxyproline (HYP) content were determined. Fibroblasts were stimulated with the BCL2 antagonist (0.01 – 100 nM). BCL2, alpha smooth muscle actin (αSMA) and collagen I (COL1A1) were determined by qPCR, IF and WB. mRNA expression pattern was determined by Next Generation Sequencing (NGS).

RESULTS: Collagen layer thickness was significantly decreased in both DSS-induced chronic colitis and the transplantation model of fibrosis upon BCL2 antagonist administration compared to vehicle. Decreased HYP content confirmed the preventive effects of the BCL2 antagonist on fibrosis. *In vitro*, a significant increase in PI^+ / annexin V^+ human colonic fibroblasts was determined by FACS upon treatment with high-dose BCL2 antagonist, at lower dose, *αSMA, COL1A1* and *TGF* were decreased. NGS, IF and qPCR revealed decreased expression and nuclear translocation of GATA6 and SOX9, known for reprogramming fibroblasts.

CONCLUSION: BCL2 antagonist administration partially prevented fibrogenesis in both fibrosis models. The BCL2 antagonist reduced the expression of TGFβ-induced factors involved in differentiation of myofibroblasts and therefore might represent a potential treatment option against CD-associated fibrosis.

Key Words: Fibroblasts; differentiation; fibrogenesis; fibrosis; intestinal; BCLXL; BCL2 family protein; BCL2 antagonist; ABT-737; treatment; transplantation; graft; TGFβ; αSMA, apoptosis

Introduction

The BCL2 family of apoptosis proteins decides over a cell´s life or death. Pro-survival BCL2 family members (BCL2, BCLXL, BCLω, BCLB, myeloid cell leukemia sequence (MCL)1 and BCL2 related protein A1) interact with pro-apoptotic BCL2 family members (e.g. BCL2 associated X (BAX), BCL2 antagonist/killer 1 (BAK), BCL2 related ovarian killer protein (BOK) from the BAX group and BCL2-like protein 11 (BIM) from the BCL2 homology (BH)3-only group), and induce or abolish apoptosis. The balance of those interactions determines the life cycle length of cells expressing the respective proteins. All pro-survival family members as well as pro-apoptotic BAX, BAK and BOK share four BH domains (1) and adopt similar structures (2). A hydrophobic surface groove is formed, a crucial interface for interactions for all pro-apoptotic BCL2 family members which share the BH3 domain necessary for dimerization and their killing activity. So-called BH3-only proteins (such as BIM) are essential for the initiation of cell death. BH3-only proteins are induced transcriptionally or post-translationally by cytotoxic stress signals. Upon these apoptotic stimuli they translocate and the BH3 amphipathic helix of BH3-only proteins binds to the hydrophobic surface groove of BCL2-like molecules, and thereby antagonise their pro-survival function (3). These interactions primarily occur on intracellular membranes, particularly the mitochondrial outer membrane (4). BAX/BAK-like proteins are further downstream in apoptosis signaling and mediate mitochondrial membrane permeabilization by forming pores in the mitochondrial membrane, which eventually leads to apoptosis (5). Pro-survival BCL2 stabilizes the mitochondrial membrane by inhibiting pore forming proteins BAX and BAK. Pro-apoptotic proteins like BIM can both antagonize the pro-survival function of BCL2 and directly bind to BAX and BAK in order to initiate apoptosis (6).

Activation and differentiation of a number of cell types, such as fibroblasts, is associated with increased cell survival, and therefore with the expression of members of the BCL2 family of proteins (7). As fibroblasts are activated during the process of fibrosis, altering BCL2 activity might be a potential treatment option. A number of BH3 mimetic small molecules like Navitoclax, Venetoclax and ABT-737 (AbbVie, USA) have been developed as potent inhibitors of pro-survival BCL2, BCLXL and BCLω (8, 9) and have been shown to disrupt the interactions of BCL2 family proteins, thereby inducing apoptosis in cancer. BCL2-specific Venetoclax was approved by the US FDA for chronic lymphocytic leukemia. ABT-737 has a high affinity to the hydrophobic surface groove of BCL2, BCLXL and BCLW but not markedly to MCL1 and A1 (4). ABT-737 inhibits BCL2 by directly blocking pro-apoptotic BIM-binding sites and displacing BIM, which becomes freely available to interact with other BCL2 molecules in the cell. Thus, BIM can bind to pro-apoptotic BAX and BAK and trigger apoptosis by initiating the formation of pores on the mitochondrial surface.

Inflammatory bowel disease (IBD) is characterized by a chronic inflammation of the intestinal wall and comprises two main conditions, namely ulcerative colitis (UC) and Crohn's disease (CD). Severe and persistent mucosal tissue damage triggers an important inflammatory response, which in turn leads to the initiation of a reparatory process (10-12). Rapid and adequate healing is essential to restore a tight barrier and reduce the exposure of the underlying tissue to luminal antigens. Excessive extracellular matrix (ECM) deposition promotes fibrosis and impairs gastrointestinal function, constituting a common clinical problem in patients with CD. Fibrosis is increasingly recognised as an important cause of morbidity and mortality in IBD. Intestinal fibrosis leads to stricture formation in 30–50% of patients with CD (13, 14), and requires surgery in approximately 80% of these patients (13).

Myofibroblasts are one of the main producers of ECM components that are deposited during fibrosis. As adequate wound healing is the result of an exquisite balance between multiple pro- and anti-fibrotic stimuli on ECM-producing fibroblasts (15-18), a decrease in fibroblast death and fibroblast differentiation into myofibroblasts have been suggested to drive fibrosis. Myofibroblasts have migratory potential, (19-21) but can also be newly generated from several sources (22), including differentiation from stem cells, transdifferentiation from fibroblasts, smooth muscle cells and stellate myofibroblasts (23).

Materials and Methods

Patients

Primary human fibroblast cultures were obtained from surgical specimens taken from healthy areas of the mucosa of a patient undergoing surgery for colorectal carcinoma or from the mucosa of patients with CD. The degree of inflammation was graded microscopically (“blind” pathologist) by determination of the inflammatory infiltrate of neutrophils, eosinophils, and lymphocytes: no inflammation, low degree of inflammation, and severe inflammation. Gender, age, clinical features and treatment of the patients are given in table 1. The study was approved by the Ethics Committee of the University of Regensburg and the University of Zurich and performed according to the Declaration of Helsinki.

Isolation and culture of human and murine intestinal fibroblasts

Human and murine intestinal fibroblasts were isolated and cultured as described previously (19). The mucosa from surgical specimens was cut into 1 mm pieces while the biopsies were used directly for the isolation of fibroblasts. Epithelial cells were removed in Hank’s Balanced Salt Solution without Ca^{2+} and Mg^{2+} (PAA, Colbe, Germany) with 2 mM EDTA (Sigma, Deisenhofen, Germany). The remaining tissue was digested for 30 minutes at 37°C with 1 mg/mL collagenase 1 (Sigma), 0.3 mg/mL DNase I (Boehringer, Mannheim, Germany), and 2 mg/mL hyaluronidase (Sigma) in PBS (Gibco, Karlsruhe, Germany). The isolated cells were cultured in 25 cm^2 culture flasks (Costar, Bodenheim, Germany) with DMEM containing 10% fetal calf serum, penicillin (100 IE/mL), streptomycin (100 µg/mL), ciprofloxacin (8 µg/mL), gentamycin (50 µg/mL), and amphotericin B (1 µg/mL). Nonadherent cells were removed.

Animals

Female B6-Tg(UBC-GFP)30Scha/J donor mice (GFP-Tg) weighing 20 g were bred locally in the animal facility of the University Hospital Zurich. C57BL/6J-Crl1 mice (C57BL/6) were obtained from Charles River. The animals received standard laboratory mouse food and water *ad libitum*. They were housed under specific pathogen-free conditions (SPF) in individually ventilated cages (IVC).

Induction and treatment of chronic dextran sulfate sodium (DSS) colitis

Female C57BL/6 weighing 20-25 g were used for the experiments and housed in IVC and under SPF for at least three weeks prior to testing. Chronic colitis was induced as described previously (24). During a cycle of chronic colitis mice received either 2.5 % DSS in drinking water or drinking water alone over seven days. In between, the animals were given 14-day periods of recovery. Mice received 3 cycles of DSS treatment as described above and were killed 2 weeks after completion of the last DSS cycle.

ABT-737 preparation and application

For *in vitro* experiments, ABT-737 was dissolved in DMSO to a stock concentration of 5 mM. For *in vivo* experiments, ABT-737 was dissolved in polyethylene glycol, Tween 80, dextrose solution and DMSO. ABT-737 was injected i.p. at a dose of 50 mg/kg/day during three cycles of DSS-induced chronic colitis. ABT-737 was injected i.p. at a dose of 50 mg/kg/day each day during two weeks in the experiment using the heterotopic intestinal transplant model.

Assessment of colonoscopy and histological score in mice

Animals were anesthetized i.p. with a mixture of 90-120 mg ketamine (Narketan 10%, Vétoquinol AG, Bern Switzerland) and 8 mg xylazine (Rompun 2%, Bayer, Switzerland) per kg body weight, and examined with the Tele Pack Pal 20043020 (Karl Storz Endoskope, Germany). Mice were scored with a murine endoscopic index of colitis severity (MEICS) as described previously (25). For the assessment of the histological scores, 1 cm of the distal third of the colon was removed and scored as described (24, 26).

Heterotopic intestinal transplant model

The heterotopic mouse intestinal transplant model is an adaption of the heterotopic transplantation model of intestinal fibrosis in rats, which has been previously described in detail (27). Briefly, donor small bowel resections were extracted and transplanted subcutaneously into the neck of recipient animals. Donor small bowel proximal to the caecum was excised and flushed with 5 ml of 0.9% NaCl to remove stool, and divided into 10 mm parts. A small bowel resection was implanted into a subcutaneous pouch, and a single dose of Cefazolin (Kefzol®, 1 g diluted in 2.5 ml aqua dest) was applied i.p. as infection prophylaxis. Intestinal grafts were explanted seven days after transplantation.

Collagen layer thickness measurement

5 µm sections were examined with the Imager Z2 (Zeiss) and the software AxioVision (Zeiss). Collagen layer thickness was determined by a blinded investigator from at least eight places in representative areas at 10-fold magnification.

HYP assay

HYP content was quantitated from freshly isolated small bowel and grafts using the HYP assay kit according to the manufacturer's protocol (MAK008-1KT, Sigma-Aldrich). In brief, tissues (10–30 mg) were homogenized using gentleMACS Octo Dissociator (130-096-427, Miltenyl Biotec) and hydrolyzed in 12 M HCl (10 µL/mg tissue). Hydrolysates were transferred in duplicate to a 96 well plate and dried at 90°C. Dried samples were incubated each with 50 µL of chloramine T/oxidation buffer mixture (3 µL of the chloramine T concentrate and 47 µL of the oxidation buffer) at room temperature for 5 minutes. 50 µL of the diluted DMAB reagent (25 µL dimethylaminobenzaldehyde, 25 µL perchloric acid/isopropanol) was subsequently added to each sample and the incubation was carried out at 60°C for 90 minutes for chromophore formation. Absorbance was read at 560 nm.

TaqMan® gene expression assays

For human: *αSMA* Hs00426835_g1, *BCL2* Hs00608023_m1, *BCLXL* Hs00236329_m1, *COL1A1* Hs00164004_m1, *COL3A1* Hs00943809_m1, *IL1β* Hs01555410_m1, *IL6* Hs00174131_m1, *MMP3* Hs00968305_m1, *MMP9* Hs00234579_m1, *TGFβ1* Hs00998133_m1, *ELN* Hs00355783_m1, *LOXL2* Hs00158757_m1, *SOX9* Hs01001343_g1, *GATA6* Hs00232018_m1, *TIMP1* Hs00171558_m1 and *GAPDH* 4326317E.

For mice: *αSma* Mm00725412_s1, *Bak1* Mm00432045_m1, *Bax* Mm00432051_m1, *Bcl2* Mm00477631_m1*, *BclXL* Mm00437783_m1, *Bim* Mm00437796_m1, *Mcl1* Mm00725832_s1*, *Mmp2* Mm00439498_m1, *Mmp3* Mm00440295_m1, *Mmp9* Mm00442991_m1, *Mmp13* Mm00439491_m1, *Tgfβ1* Mm01178820_m1, *Timp1* Mm00441818_m1, *Loxl2* Mm00804740_m1, *Col1a1* Mm00801666_g1, *Col3a1* Mm01254476_m1, *Il6* Mm00446190_m1 *Ifnβ* Mm00439552_s1, Ifnγ

Mm00801778_m1, *Il10* Mm00439615_g1, *Tnf* Mm00443259_g1 and *Gapdh* 4352339E. Relative gene expression was calculated using the ΔΔCt-method.

Cell viability assay

5000 cells per well were grown in triplicate in 96-well plates. Cells were starved for 24h before stimulation. Colorimetric assay (CK04; Dojindo Molecular Technologies) was performed according to the manufacturer's protocol.

Cell death assays

Caspase-3/7 activity was quantified using the fluorogenic Ac-DEVD-AMC substrate (Enzo Life Sciences, Farmingdale, NY). Briefly, cells were grown in black 96-well plates with clear bottoms with respective treatments. 2x lysis buffer (100 mM HEPES, pH 7.4, 200 mM NaCl, 0.2% CHAPS, 2 mM DTT, 0.2 mM EDTA) was added to each well and incubated for 15 min at 4°C. Caspase assay buffer (50 mM HEPES, pH 7.4, 100 mM NaCl, 0.1% CHAPS, 1 mM DTT, 0.1 mM EDTA, 10% glycerol) containing Ac-DEVD-AMC (final 50 µM) was added to each well and release of AMC was measured after 1 hour incubation at 37°C using a fluorescence microplate reader (Synergy 2, BioTek, Winooski, VT; excitation 360 nm, emission 460 nm).

Numbers of living and apoptotic fibroblasts were determined by flow cytometry of annexin V- and propidium iodide (PI)-stained fibroblasts. Fibroblasts were resuspended in annexin V binding buffer, as indicated by the manufacturer, and stained with allophycocyanin (APC)-conjugated annexin V (Enzo Life Science, Basel, Switzerland; diluted 1 : 40) and PI (Sigma-Aldrich, St Louis, MO, USA; final concentration 25 mg/ml). Annexin V^-/PI^- cells were considered alive; apoptotic cells displayed staining for annexin V and PI. Fluorescence was measured by flow cytometry

using a BD fluorescence activated cell sorter (FACS)Canto II flow cytometer equipped with two lasers (excitation wave lengths: 488 and 633 nm).

For IHC staining of formalin-fixed paraffin-embedded tissue samples, antigen retrieval was carried out using Cell Conditioning 1 (950-124, Ventana) for 90 min. Pre-treated tissue samples were incubated with the cleaved caspase-3 antibody (1:300 dilution, #9661, Cell Signaling Technology) for 44 min. Reactions were carried out on Benchmark Discovery (Ventana). For IHC staining of human fibroblast cultures, the same procedure was carried out as described above without antigen retrieval. Cleaved caspase-3 antibody was diluted 1:200 before usage.

Next generation sequencing (NGS)

Primary human colonic fibroblasts were stimulated either with vehicle or 5 ng/ml recombinant TGFβ in the presence or absence of 10 nM ABT-737. Two independent experiments were performed and NGS was performed using total RNA that passed Tapestation (Agilent) quality control (RIN > 8.3). Illumina NGS was performed by the Functional Genomics Center Zurich. For further analyses STRING software according to the PathCards from the Weizmann Institute of Science was used. Kyoto Encyclopedia of Genes and Genomes (KEGG) pathway analyses revealed genes from the TGFβ signaling pathway to be increased > 2-fold upon recombinant TGFβ and decreased > 2-fold upon additional ABT-737. KEGG signaling pathway analyses “regulation of stem cell differentiation”, “regulation of cell development” and “regulation of cell differentiation” were applied.

Western blot

Western blots were performed using goat anti-mouse αSMA (PA5-18292, Thermo Fisher Scientific), rabbit anti-human Bcl2 (#2870, Cell Signaling Technology), rabbit anti-human BclXL (#2764, Cell signaling Technology), rabbit anti-mouse βactin (#4970, Cell Signaling Technology), horseradish peroxidase-conjugated secondary antibody goat anti-rabbit (#sc-2004, Santa Cruz) and horseradish peroxidase-conjugated secondary antibody donkey anti-goat (#sc-2020, Santa Cruz). Luminescence was quantified using ImageJ.

Statistical analysis

Statistical analysis was performed using Kruskal-Wallis one-way analysis of variance (ANOVA) on ranks, all pairwise multiple comparison procedures, Tukey's test, Holm-Sidak method or unpaired t-test, as indicated. Differences were considered significant at a *p*-value of < 0.05 and highly significant at a *p*-value of < 0.01 and *p*-value of < 0.001.

Ethical considerations

Experiments with human primary fibroblasts were approved by the local ethical committees (EK-1316).

The experimental protocol was approved by the local Animal Care Committee of the University of Zurich (registration number ZH183/2014).

Results

The BCL2 antagonist reduced fibrosis in DSS-induced chronic colitis

We investigated whether BCL2 antagonist administration reduces fibrosis in the model of DSS-induced chronic colitis (n = 39 mice). Successful induction of colitis was confirmed by an intermittent body weight loss, a significant increase in spleen weight, and shortening of the colon compared to water control (supplementary figure 1). Due to its known anti-inflammatory properties, BCL2 antagonist was efficacious in ameliorating colitis confirmed by a significantly decreased MEICS, a decreased histological score, and a reduction in the mRNA expression of *Ifnγ* and *Tnf* compared to vehicle-treated mice (supplementary figure 2).

To determine fibrosis, we performed Sirius red staining to assess collagen deposition. Mice without DSS-induced colitis displayed a normal collagen layer thickness in the colon of both vehicle- and BCL2 antagonist-treated mice (figure 1A). During DSS administration, collagen deposition was significantly increased compared to water controls. Microscopy evidenced a significant decrease in collagen layer thickness in the colon from mice treated with the BCL2 antagonist in comparison to colon from vehicle-treated mice (figure 1A). HYP assay confirmed that the BCL2 antagonist significantly decreased collagen deposition in comparison to vehicle-treated mice (figure 1B). IHC staining of colon histological cross sections revealed an increase in cleaved caspase 3 positive foci in the lamina propria and Peyer's patches upon treatment with the pro-apoptotic BCL2 antagonist compared to vehicle in DSS-induced colitis (figure 1C). Transcriptional expression of *αSma* and *Tgf* was decreased in colon from BCL2 antagonist-treated mice compared to vehicle-treated mice (figure 1D), in contrast, tissue inhibitor of metalloproteinase (*Timp)1* was increased in colon from BCL2 antagonist-treated mice compared to vehicle-treated mice (figure 1D).

The BCL2 antagonist reduced fibrosis in the transplantation model of fibrosis

We next investigated whether BCL2 antagonist administration would also reduce fibrosis in the heterotopic transplantation mouse model of intestinal fibrosis (n = 25 mice). Stained histological cross sections from freshly isolated small intestine showed an open lumen and distinctive epithelial crypts. Seven days after transplantation, the lumen of intestinal grafts was obstructed by granulation and fibrotic tissue (figure 2A). Epithelial structure was almost lost in heterotopic intestinal isografts. Microscopy evidenced a decrease in collagen deposition in freshly isolated small bowel and in intestinal transplants upon treatment with the BCL2 antagonist compared to vehicle under polarizing light and transmission light. Collagen layer thickness was significantly decreased in harvested grafts from mice upon treatment with the BCL2 antagonist in comparison to grafts from vehicle-treated mice for both polarizing light (figure 2A) and transmission light (supplementary figure 3). HYP assay confirmed that BCL2 antagonist treatment significantly decreased collagen content in comparison to vehicle-treated mice (figure 2B).

Heterotopic transplantation of small bowel resections in mice was followed by a significant increase in the mRNA expression of both *Col1a1* and *Col3a1* compared to freshly isolated small bowel (figure 2C). The grafts showed a trend towards a decreased *Col1a1* and *Col3a1* mRNA expression upon administration of the BCL2 antagonist compared to vehicle. Next, we determined the expression of *Mmp2* and *Timp1* in intestinal transplants by qPCR. Transplantation was followed by a significant increase in *Mmp2* (figure 2C). Grafts from mice treated with the BCL2 antagonist showed a trend towards a decreased *Mmp2* expression compared to vehicle. In contrast, tissue inhibitor *Timp1* was increased upon treatment with BCL2 antagonist.

Treatment with BCL2 antagonist decreases the differentiation of murine myofibroblasts

Next, we sought to determine the impact of BCL2 antagonist treatment on the differentiation of primary murine colonic fibroblasts. Cell viability remained unchanged in murine fibroblasts following TGFβ-stimulation and administration of the BCL2 antagonist (figure 3A). TGFβ-induced transcriptional expression of *αSma* decreased in a dose-dependent manner in the presence of the BCL2 antagonist indicating that the BCL2 antagonist hinders fibroblast proliferation (figure 3B). Western blot analysis revealed significantly increased αSMA protein levels in the presence of TGFβ, but a dose-dependent decrease in αSMA upon BCL2 antagonist treatment (figure 3C). IF analysis confirmed a decrease in αSMA protein upon BCL2 antagonist treatment in the absence (figure 3D) or presence of TGFβ (figure 3E).

TGFβ also significantly increased mRNA expression of the structural protein *Col1a1* in primary murine fibroblasts compared to fibroblasts without TGFβ stimulation (figure 4A). Conversely, *Col1a1* and *Col3a1* expression was decreased upon BCL2 antagonist treatment in a dose-dependent manner (figure 4A). TGFβ significantly increased collagen crosslinking enzyme *Loxl2,* a crucial protein for the stabilization of collagen fibrils and fibers in the ECM (figure 4B). The BCL2 antagonist significantly decreased TGFβ-induced *Loxl2* in a dose-dependent manner (figure 4B).

Similarly, TGFβ-induced *Timp1* expression decreased upon BCL2 antagonist treatment (figure 4C). Following TGFβ stimulation, mRNA of ECM-degrading enzymes *Mmp3* and *Mmp9* increased (supplementary figure 4A and B). *Mmp3* decreased upon high-dose BCL2 antagonist treatment (supplementary figure 4A), but *Mmp9* increased in the presence of the BCL2 antagonist (supplementary figure 4B). *Mmp13* was not affected by TGFβ or BCL2 antagonist (supplementary figure 4C).

Next, we analyzed the mRNA expression of pro- and anti-inflammatory cytokines upon TGFβ-induced differentiation of murine fibroblasts in the presence of the BCL2 antagonist. Stimulation with TGFβ significantly increased endogenous *Tgfβ*, which acts as an anti-inflammatory and pro-fibrotic cytokine (figure 4D). The BCL2 antagonist significantly decreased *Tgfβ* in a dose-dependent manner. Anti-inflammatory *Il10* was not detectable in fibroblasts regardless of TGFβ and BCL2 antagonist stimulation (not shown). Pro-inflammatory *Il6* was significantly increased following TGFβ treatment, and significantly decreased in the presence of the BCL2 antagonist (figure 4E). Pro-inflammatory *Ifnγ* was not detectable in fibroblasts regardless of TGFβ and BCL2 antagonist stimulation (not shown).

Further, we analysed the mRNA expression of members of the BCL2 family of apoptosis proteins. Pro-survival *BclXL*, *Bcl2* and *Mcl1* were not regulated following TGFβ stimulation (supplementary figure 5A). *BclXL* increased following administration of BCL2 antagonist in a dose-dependent manner compared to vehicle. Pro-apoptotic *Bim*, *Bak and Bax* were not regulated in the presence or absence of TGFβ and the BCL2 antagonist stimulation (supplementary figure 5B).

Additionally, in the murine 3T3 fibroblast cell line TGFβ-mediated *Mmp3* and *Il6* mRNA expression was reduced in the presence of the BCL2 antagonist confirming the results obtained with primary murine fibroblasts (supplementary figure 6). *Il10* and *Ifnγ* were not detectable in 3T3 regardless of TGFβ and BCL2 antagonist stimulation (not shown).

Treatment with the BCL2 antagonist decreased differentiation of human myofibroblasts

Next, we determined the impact of BCL2 antagonist treatment on differentiation of primary human colonic fibroblasts. Cell viability increased following TGFβ stimulation in human fibroblasts and showed a trend towards a decrease upon administration of BCL2 antagonist (figure 5A). Accordingly, caspase 3/7 activity showed a trend towards an increase upon BCL2 antagonist treatment (figure 5B). The presence of cleaved caspase 3 positive fibroblasts upon treatment with high-dose BCL2 antagonist was confirmed by IHC (figure 5C). A significant increase in PI^+ / annexin V^+ human colonic fibroblasts was determined by flow cytometry upon treatment with high-dose BCL2 antagonist (figure 5D).

To elucidate whether TGF-β-mediated differentiation of human fibroblasts is decreased upon BCL2 antagonist treatment, αSMA expression was analyzed. Transcriptional expression of *αSMA* was significantly increased upon TGFβ treatment but decreased in the presence of the BCL2 antagonist (figure 6A, supplementary figure 7A, patient 2). Furthermore, IF analysis showed a decrease of αSMA protein upon antagonist treatment (figure 6B). Similarly, TGFβ-induced *COL1A1*, *COL3A1* and *TGFβ mRNA expression* decreased upon antagonist treatment in human fibroblasts (figure 6C and D, supplementary figure 7B and C, patient 2). Elastin mRNA (*ELN*) decreased upon BCL2 antagonist treatment (supplementary figure 8A, patient 2), whereas *LOXL2* remained unchanged regardless of TGFβ and BCL2 antagonist stimulation (supplementary figure 8B, patient 2). *MMP3*, *MMP9* and *TIMP1* did not change significantly upon BCL2 antagonist treatment (supplementary figure 9A and B). *MMP13*, *IL6*, *IFNγ* and *IL10* were not detectable in human primary fibroblasts regardless of TGFβ and BCL2 stimulation (not shown).

We next determined the effects of the BCL2 antagonist on the expression of BCLXL and BCL2 in primary human colonic fibroblasts. *BCLXL* mRNA remained unchanged in the presence of both TGFβ and the BCL2 antagonist (supplementary figure 10A). In contrast, BCL2 protein decreased upon BCL2 antagonist treatment as shown by Western blot (figure 7A). *BCL2* mRNA was decreased following TGFβ stimulation and increased upon antagonist treatment, but not significantly (supplementary figure 10B, C). In contrast, Western blot revealed a decrease in BCL2 protein upon BCL2 antagonist treatment (figure 7B).

Treatment with the BCL2 antagonist decreased nuclear translocation of GATA6 and pSOX9

We determined the effects of BCL2 antagonist treatment on the mRNA expression pattern in primary human colonic fibroblasts by NGS. A total of 20400 genes were identified. Following TGFβ stimulation, 844 genes were increased > 2-fold compared to vehicle in two independent experimental rounds. Upon additional stimulation with the BCL2 antagonist, 247 of these genes were decreased > 2-fold compared to TGFβ stimulation alone in both experimental rounds (figure 8A and supplementary table). Regulated genes include a number of cytoskeletal proteins and ECM components (ACTB, ACTC1, ACTG2, COL1A1, COL16A1, COL4A3, COMP, ELN, EMILIN2, FIBCD1). KEGG analyses revealed regulated genes from the TGFβ signaling pathway (TGFB2, THBS1, LEFTY2, NOG, CDKN2B), and the transcription factors GATA binding protein 6 (GATA6) and SRY-Box 9 (SOX9).

GATA6 performs its biological activity after being phosphorylated and translocated to the nucleus, but an anti-pGATA6 ab is not commercially available. On the other hand, total GATA6 expression is induced by TGFβ during myofibroblast differentiation. Therefore, we performed qPCR and IF using anti-GATA6 ab. TGFβ stimulation

significantly increased *GATA6* in human fibroblasts compared to vehicle (figure 8B) but expression decreased in the presence of the BCL2 antagonist. GATA6 protein was detected in human fibroblasts regardless of TGFβ stimulation (figure 8C) and was decreased upon BCL2 antagonist treatment.

TGFβ-induced *SOX9* mRNA expression was decreased upon BCL2 antagonist stimulation compared to vehicle in human fibroblasts (figure 8B). Anti-pSOX9 ab did not work on human fibroblasts, but showed cross-reactivity on primary murine fibroblasts. pSOX9 was detected in the nuclei of murine fibroblasts upon TGF-β treatment, but the antagonist decreased pSOX9 in a dose-dependent manner (figure 8D). Similarly, the BCL2 antagonist decreased TGFβ-mediated SOX9 accumulation in the nuclei of human fibroblasts (figure 8E).

Discussion

In the present study, we show that the BCL2 antagonist ABT-737 hindered the development of intestinal fibrosis in both the DSS mouse model of chronic colitis and the mouse heterotopic transplantation model of fibrosis, indicated by a significant decrease in collagen mRNA expression, collagen layer thickness and HYP content. Interestingly, pro-apoptotic ABT-737 also has anti-inflammatory properties. Recent studies showed that the BCL2 antagonist has a direct effect on activated lymphocytes. The BCL2 family plays a critical role in controlling immune responses by regulating the expansion and contraction of the activated lymphocyte population via apoptosis (28-32). In IBD, the inflammatory state is sustained by an exaggerated response of T-lymphocytes to luminal antigens associated with an increased resistance to apoptosis (31). ABT-737 is effective in limiting the persistence of lymphocytes in spontaneous mouse models of colitis (33). Regulation of inappropriate survival of lymphocytes by ABT-737 is also effective in treating animal models of autoimmune diseases (34), arthritis (35) and lupus (36). Consequently, regulation of inappropriate survival of lymphocytes by the BCL2 antagonist may also represent a therapeutic anti-inflammatory strategy in IBD.

In the model of DSS-induced chronic colitis, fibrosis is induced through a recurrent damage of the integrity of the mucosal barrier resulting in long-running lymphocyte infiltration and chronic colitis. At first hand, ABT-737 could decrease inflammation over time, thereby limiting the basis for the initiation of fibrosis. In experiments presented in this work, this is evidenced by increased apoptosis in Peyer's patches and the *lamina propria*, and a decrease in the expression of pro-inflammatory cytokines. Targeting BCL2 family proteins to initiate lymphocyte apoptosis may contribute to decreased fibrogenesis, but BCL2 antagonists could also have a more wide effect on fibroblast

differentiation. The BCL2 antagonist is also effective to reduce fibrosis in the much faster heterotopic transplantation mouse model of intestinal fibrosis, characterized by increased TGFβ levels, hypoxia and neovascularization of the fibrotic graft. We could also demonstrate anti-fibrotic effects of the BCL2 antagonist on murine and human colonic fibroblasts. High concentrations of ABT-737 induce apoptosis in colonic fibroblasts *in vitro* as shown by caspase activity assay, cleaved caspase 3 IHC and flow cytometry. The BCL2 antagonist ABT-737 shows a potent action against various transformed cells while exhibiting minimal toxicity toward normal cells, e.g. intestinal epithelial cells (37). Results from our *in vitro* experiments showed that the BCL2 antagonist does not alter intestinal fibroblast viability at low concentrations, but still reverses TGFβ mediated effects. Hallmarks of fibroblast differentiation and fibrogenesis, such as increased expression of αSMA and *COL1A1* are inhibited upon BCL2 antagonist treatment.

A reasonable number of genes for cytoskeletal proteins and ECM components were shown to be inhibited upon BCL2 antagonist treatment compared to vehicle. However, ECM-degrading MMPs and TIMP1 were shown to be regulated paradoxically. The interaction between MMPs and TIMP1 is highly controlled and characterized by an interplay of increased and declined expression (reviewed in (38) for liver fibrosis). Expression levels may vary depending on the time point for data collection, scheduled after several weeks for *in vivo* experiments compared to a 24h stimulation for cell lines. Differentiation of colonic fibroblasts is considered a main driving factor in intestinal fibrosis. Myofibroblasts, representing the activated phenotype, can differentiate from stem cells (22) or be newly generated by trans-differentiation from fibroblasts, smooth muscle cells and stellate myofibroblasts (23). We could show a decrease in the expression and nuclear translocation of the transcription factors GATA6 and SOX9 upon BCL2 antagonist treatment in primary intestinal fibroblasts. GATA6 has been

previously shown to participate in the differentiation of fibroblasts into myofibroblasts in idiopathic pulmonary fibrosis (IPF) lungs (39). The inhibition of GATA-6 in lung fibroblasts showed that the transcription factor mediates aSMA–induction upon TGFβ stimulation. SOX9 has been identified as an important link between differentiation, proliferation and apoptosis in rat mesenchymal stem cells (40). SOX9 modulates BCL2-dependent apoptosis in undifferentiated adult mesenchymal stem cells, emphasizing the importance for successful repair and regeneration in tissues and organs in adults. Taken together these results point to that BCL2 antagonist treatment reduces progressive differentiation of human intestinal fibroblasts into myofibroblasts. Intestinal fibrosis is viewed as a unidirectional process consisting of a chronic response of the digestive tract, in which inflammation induces local fibroblasts to multiply, become activated and deposit extracellular matrix proteins as part of the wound healing process (41). There is evidence that intestinal fibrogenesis, once initiated, is self-perpetuating (42) and constitutes a very early process associated with inflammation (43). Results from our own studies support this hypothesis as we determined a rapid increase of collagen layer thickness and rapid increase of TGFβ in grafts shortly after transplantation (44). Administration of anti-inflammatory agents effectively treats inflammatory flares, but may not be able to alter the course of intestinal fibrosis and prevent the formation of strictures (45, 46). Despite earlier initiation of immunosuppressants or biologicals during the course of CD, the percentage of patients requiring intestinal surgery due to the occurrence of stricturing complications has only decreased slightly (47). But potent anti-inflammatory agents alone may not prevent fibroblast recruitment and differentiation.

Activation and differentiation of fibroblasts is linked to the expression of members of the BCL2 family of proteins, and there is a particular interest in the development of

inhibitors of the BCL2 family for the treatment of fibrotic diseases. We could show a decrease in BCL2 and BCLXL upon BCL2 antagonist compared to vehicle. However, qPCR showed a trend to increased murine *BclXL*, human *BCL2* and *BCLXL* what could be a compensation of decreased protein level. There is strong evidence that antagonizing pro-survival BCL2 family members induces apoptosis in activated fibroblasts but not in quiescent fibroblasts. Thus, selective inhibition of BCLXL by A-1331852 or BCLXL-specific siRNA silencing induced apoptosis in activated fibroblasts but had no effect on quiescent fibroblasts (48). Treatment with A-1331852 resulted in a significant reduction of liver fibrosis in a murine model of biliary fibrosis, possibly as a result of a dual effect on activated fibroblasts and senescent cholangiocytes. Cardiac fibrosis has been partially prevented through microRNA-21-mediated decrease of *BCL2* in cultured cardiac fibroblasts and in a rat model of cardiac fibrosis (49). Dermal myofibroblasts isolated from patients with systemic sclerosis show increased *BCL2* compared to fibroblasts from control subjects Decreasing *BCL2* using microRNA-29a increased apoptosis in dermal fibroblasts (50).

Further, there is extensive literature on myofibroblast apoptosis resistance being associated with the progression of IPF (51). Pathologic lesions called “fibroblastic foci” have been associated with IPF (52) and are characterized by prominent epithelial cell apoptosis but insufficient mesenchymal cell apoptosis (53, 54). While there is no robust fibroblast proliferation within fibroblast foci (39, 55), decreased fibroblast apoptosis has been suggested as a mechanism underlying the accumulation of these cells (55, 56). Fibroblastic foci were positive for the transcription factor GATA6, but negative for Ki67 and caspase 3 confirming the absence of apoptosis (39). TGFβ and endothelin-1 promote myofibroblast apoptosis resistance via activation of focal adhesion kinase and PI3K/AKT signaling pathways (57, 58), which in turn induce the expression of anti-

apoptotic X-linked inhibitor of apoptosis and survivin, which are increased in fibroblast foci of IPF tissue (59, 60). Additionally, myofibroblasts isolated from lungs of patients suffering from IPF show increased *BCL2* compared to fibroblasts from control subjects (61). Decreasing *Bcl2* during the post-inflammatory fibrotic phase of lung injury protects mice from experimental lung fibrosis (61).

In summary, we showed that low concentrations of the antagonist of pro-apoptotic BCL2 prevents fibroblast activation and differentiation of fibroblasts into myofibroblasts. High concentrations induce apoptosis in fibroblasts. ABT-737 partially prevents intestinal fibrogenesis in the DSS-induced model of colitis and in a heterotopic transplantation model of fibrosis. BCL2 antagonists may therefore represent a new treatment option to prevent fibrogenesis in IBD patients, and to reduce colitis through the reduction of lymphocytes.

References

1. Kvansakul M, Yang H, Fairlie WD, et al. Vaccinia virus anti-apoptotic F1L is a novel Bcl-2-like domain-swapped dimer that binds a highly selective subset of BH3-containing death ligands. Cell death and differentiation. 2008;15:1564-1571

2. Muchmore SW, Sattler M, Liang H, et al. X-ray and NMR structure of human Bcl-xL, an inhibitor of programmed cell death. Nature. 1996;381:335-341

3. Cory S, Adams JM. The Bcl2 family: regulators of the cellular life-or-death switch. Nat Rev Cancer. 2002;2:647-656

4. Czabotar PE, Lessene G, Strasser A, et al. Control of apoptosis by the BCL-2 protein family: implications for physiology and therapy. Nature reviews Molecular cell biology. 2014;15:49-63

5. Labi V, Erlacher M, Kiessling S, et al. BH3-only proteins in cell death initiation, malignant disease and anticancer therapy. Cell death and differentiation. 2006;13:1325-1338

6. Merino D, Giam M, Hughes PD, et al. The role of BH3-only protein Bim extends beyond inhibiting Bcl-2-like prosurvival proteins. The Journal of cell biology. 2009;186:355-362

7. Kis K, Liu X, Hagood JS. Myofibroblast differentiation and survival in fibrotic disease. Expert reviews in molecular medicine. 2011;13:e27

8. Oltersdorf T, Elmore SW, Shoemaker AR, et al. An inhibitor of Bcl-2 family proteins induces regression of solid tumours. Nature. 2005;435:677-681

9. Chen S, Dai Y, Pei XY, et al. Bim upregulation by histone deacetylase inhibitors mediates interactions with the Bcl-2 antagonist ABT-737: evidence for distinct roles for Bcl-2, Bcl-xL, and Mcl-1. Mol Cell Biol. 2009;29:6149-6169

10. Jones MK, Tomikawa M, Mohajer B, et al. Gastrointestinal mucosal regeneration: role of growth factors. Front Biosci. 1999;4:D303-309

11. Rieder F, Brenmoehl J, Leeb S, et al. Wound healing and fibrosis in intestinal disease. Gut. 2007;56:130-139

12. Sartor RB. Current concepts of the etiology and pathogenesis of ulcerative colitis and Crohn's disease. Gastroenterology clinics of North America. 1995;24:475-507

13. Cosnes J, Cattan S, Blain A, et al. Long-term evolution of disease behavior of Crohn's disease. Inflammatory bowel diseases. 2002;8:244-250

14. Freeman HJ. Natural history and clinical behavior of Crohn's disease extending beyond two decades. J Clin Gastroenterol. 2003;37:216-219

15. Pardo A, Selman M. Matrix metalloproteases in aberrant fibrotic tissue remodeling. Proceedings of the American Thoracic Society. 2006;3:383-388

16. Kim H, Oda T, Lopez-Guisa J, et al. TIMP-1 deficiency does not attenuate interstitial fibrosis in obstructive nephropathy. Journal of the American Society of Nephrology : JASN. 2001;12:736-748

17. Underwood DC, Osborn RR, Bochnowicz S, et al. SB 239063, a p38 MAPK inhibitor, reduces neutrophilia, inflammatory cytokines, MMP-9, and fibrosis in lung. American journal of physiology Lung cellular and molecular physiology. 2000;279:L895-902

18. Vaillant B, Chiaramonte MG, Cheever AW, et al. Regulation of hepatic fibrosis and extracellular matrix genes by the th response: new insight into the role of tissue inhibitors of matrix metalloproteinases. Journal of immunology. 2001;167:7017-7026

19. Leeb SN, Vogl D, Falk W, et al. Regulation of migration of human colonic myofibroblasts. Growth Factors. 2002;20:81-91

20. Di Sabatino A, Jackson CL, Pickard KM, et al. Transforming growth factor beta signalling and matrix metalloproteinases in the mucosa overlying Crohn's disease strictures. Gut. 2009;58:777-789

21. Meier JK, Scharl M, Miller SN, et al. Specific differences in migratory function of myofibroblasts isolated from Crohn's disease fistulae and strictures. Inflammatory bowel diseases. 2011;17:202-212

22. Bucala R, Spiegel LA, Chesney J, et al. Circulating fibrocytes define a new leukocyte subpopulation that mediates tissue repair. Molecular medicine. 1994;1:71-81

23. Powell DW, Mifflin RC, Valentich JD, et al. Myofibroblasts. I. Paracrine cells important in health and disease. The American journal of physiology. 1999;277:C1-9

24. Obermeier F, Kojouharoff G, Hans W, et al. Interferon-gamma (IFN-gamma)- and tumour necrosis factor (TNF)-induced nitric oxide as toxic effector molecule in chronic dextran sulphate sodium (DSS)-induced colitis in mice. Clin Exp Immunol. 1999;116:238-245

25. Becker C, Fantini MC, Wirtz S, et al. In vivo imaging of colitis and colon cancer development in mice using high resolution chromoendoscopy. Gut. 2005;54:950-954

26. Steidler L, Hans W, Schotte L, et al. Treatment of murine colitis by Lactococcus lactis secreting interleukin-10. Science. 2000;289:1352-1355

27. Hausmann M, Rechsteiner T, Caj M, et al. A new heterotopic transplant animal model of intestinal fibrosis. Inflammatory bowel diseases. 2013;19:2302-2314

28. Mitchell T, Kappler J, Marrack P. Bystander virus infection prolongs activated T cell survival. J Immunol. 1999;162:4527-4535

29. Hildeman DA, Zhu Y, Mitchell TC, et al. Activated T cell death in vivo mediated by proapoptotic bcl-2 family member bim. Immunity. 2002;16:759-767

30. Boirivant M, Marini M, Di Felice G, et al. Lamina propria T cells in Crohn's disease and other gastrointestinal inflammation show defective CD2 pathway-induced apoptosis. Gastroenterology. 1999;116:557-565

31. Ina K, Itoh J, Fukushima K, et al. Resistance of Crohn's disease T cells to multiple apoptotic signals is associated with a Bcl-2/Bax mucosal imbalance. J Immunol. 1999;163:1081-1090

32. Itoh J, de La Motte C, Strong SA, et al. Decreased Bax expression by mucosal T cells favours resistance to apoptosis in Crohn's disease. Gut. 2001;49:35-41

33. Lutz C, Mozaffari M, Tosevski V, et al. Increased lymphocyte apoptosis in mouse models of colitis upon ABT-737 treatment is dependent upon BIM expression. Clin Exp Immunol. 2015;181:343-356

34. Bardwell PD, Gu J, McCarthy D, et al. The Bcl-2 family antagonist ABT-737 significantly inhibits multiple animal models of autoimmunity. J Immunol. 2009;182:7482-7489

35. Liu H, Pope RM. The role of apoptosis in rheumatoid arthritis. Curr Opin Pharmacol. 2003;3:317-322

36. Nagy G, Koncz A, Perl A. T- and B-cell abnormalities in systemic lupus erythematosus. Crit Rev Immunol. 2005;25:123-140

37. Cippa PE, Kraus AK, Edenhofer I, et al. The BH3-mimetic ABT-737 inhibits allogeneic immune responses. Transpl Int. 2011;24:722-732

38. Hemmann S, Graf J, Roderfeld M, et al. Expression of MMPs and TIMPs in liver fibrosis - a systematic review with special emphasis on anti-fibrotic strategies. J Hepatol. 2007;46:955-975

39. Lepparanta O, Pulkkinen V, Koli K, et al. Transcription factor GATA-6 is expressed in quiescent myofibroblasts in idiopathic pulmonary fibrosis. American journal of respiratory cell and molecular biology. 2010;42:626-632

40. Stockl S, Bauer RJ, Bosserhoff AK, et al. Sox9 modulates cell survival and adipogenic differentiation of multipotent adult rat mesenchymal stem cells. J Cell Sci. 2013;126:2890-2902

41. M. P. Fibrosis in the GI tract: pathophysiology, diagnosis and treatment options. Front Gastrointest Res. 2010;26:15-31

42. Johnson LA, Luke A, Sauder K, et al. Intestinal fibrosis is reduced by early elimination of inflammation in a mouse model of IBD: impact of a "Top-Down" approach to intestinal fibrosis in mice. Inflammatory bowel diseases. 2012;18:460-471

43. Rieder F, Kessler S, Sans M, et al. Animal models of intestinal fibrosis: new tools for the understanding of pathogenesis and therapy of human disease. Am J Physiol Gastrointest Liver Physiol. 2012;303:G786-801

44. Meier R, Lutz C, Cosin-Roger J, et al. Decreased Fibrogenesis After Treatment with Pirfenidone in a Newly Developed Mouse Model of Intestinal Fibrosis. Inflammatory bowel diseases. 2016;22:569-582

45. D'Haens G, Geboes K, Rutgeerts P. Endoscopic and histologic healing of Crohn's (ileo-) colitis with azathioprine. Gastrointestinal endoscopy. 1999;50:667-671

46. Vermeire S, van Assche G, Rutgeerts P. Review article: Altering the natural history of Crohn's disease--evidence for and against current therapies. Alimentary pharmacology & therapeutics. 2007;25:3-12

47. Cosnes J, Nion-Larmurier I, Beaugerie L, et al. Impact of the increasing use of immunosuppressants in Crohn's disease on the need for intestinal surgery. Gut. 2005;54:237-241

48. Moncsek A, Al-Suraih MS, Trussoni CE, et al. Targeting senescent cholangiocytes and activated fibroblasts with Bcl-xL inhibitors ameliorates fibrosis in Mdr2-/- mice. Hepatology. 2017

49. Dong S, Ma W, Hao B, et al. microRNA-21 promotes cardiac fibrosis and development of heart failure with preserved left ventricular ejection fraction by up-regulating Bcl-2. International journal of clinical and experimental pathology. 2014;7:565-574

50. Jafarinejad-Farsangi S, Farazmand A, Mahmoudi M, et al. MicroRNA-29a induces apoptosis via increasing the Bax:Bcl-2 ratio in dermal fibroblasts of patients with systemic sclerosis. Autoimmunity. 2015;48:369-378

51. Huang SK, Horowitz JC. Outstaying their Welcome: The Persistent Myofibroblast in IPF. Austin journal of pulmonary and respiratory medicine. 2014;1:3

52. Horowitz JC, Thannickal VJ. Epithelial-mesenchymal interactions in pulmonary fibrosis. Seminars in respiratory and critical care medicine. 2006;27:600-612

53. Thannickal VJ, Horowitz JC. Evolving concepts of apoptosis in idiopathic pulmonary fibrosis. Proceedings of the American Thoracic Society. 2006;3:350-356

54. Horowitz JC, Peters-Golden M. Prostaglandin E2's new trick: "decider" of differential alveolar cell life and death. American journal of respiratory and critical care medicine. 2010;182:2-3

55. Cha SI, Groshong SD, Frankel SK, et al. Compartmentalized expression of c-FLIP in lung tissues of patients with idiopathic pulmonary fibrosis. American journal of respiratory cell and molecular biology. 2010;42:140-148

56. Korfei M, Ruppert C, Mahavadi P, et al. Epithelial endoplasmic reticulum stress and apoptosis in sporadic idiopathic pulmonary fibrosis. American journal of respiratory and critical care medicine. 2008;178:838-846

57. Horowitz JC, Lee DY, Waghray M, et al. Activation of the pro-survival phosphatidylinositol 3-kinase/AKT pathway by transforming growth factor-beta1 in mesenchymal cells is mediated by p38 MAPK-dependent induction of an autocrine growth factor. The Journal of biological chemistry. 2004;279:1359-1367

58. Horowitz JC, Rogers DS, Sharma V, et al. Combinatorial activation of FAK and AKT by transforming growth factor-beta1 confers an anoikis-resistant phenotype to myofibroblasts. Cellular signalling. 2007;19:761-771

59. Ajayi IO, Sisson TH, Higgins PD, et al. X-linked inhibitor of apoptosis regulates lung fibroblast resistance to Fas-mediated apoptosis. American journal of respiratory cell and molecular biology. 2013;49:86-95

60. Horowitz JC, Ajayi IO, Kulasekaran P, et al. Survivin expression induced by endothelin-1 promotes myofibroblast resistance to apoptosis. The international journal of biochemistry & cell biology. 2012;44:158-169

61. Zhou Y, Huang X, Hecker L, et al. Inhibition of mechanosensitive signaling in myofibroblasts ameliorates experimental pulmonary fibrosis. The Journal of clinical investigation. 2013;123:1096-1108

Figure legends

Figure 1: **The BCL2 antagonist reduces fibrosis in DSS-induced chronic colitis.** Mice received 3 cycles of DSS treatment and were killed 2 weeks after completion of the last cycle. BCL2 antagonist was injected during three cycles of DSS-induced chronic colitis. (A) Sirius red staining. Transmission light microscopy confirmed significantly decreased collagen layer thickness upon BCL2 antagonist treatment compared to vehicle. Thickness was calculated from at least eight places in representative areas at 10-fold magnification for each single tissue sample. Mean value and standard deviation are shown. (B) HYP assay. (C) Cleaved caspase 3 IHC. (D) qPCR for *αSma*, *Tgf* and *Timp1* (* $p < 0.05$, ** $p < 0.01$, ANOVA, t-test).

Figure 2: **BCL2 antagonist administration significantly reduces collagen layer thickness in grafts from the heterotopic transplantation model.** BCL2 antagonist was injected each day during two weeks in the experiment. (A) Sirius Red staining. Polarizing light microscopy confirmed significantly decreased collagen layer thickness upon treatment with the BCL2 antagonist compared to vehicle. Thickness was calculated from at least eight places in representative areas at 10-fold magnification for each single graft. Mean value and standard deviation are shown. (B) HYP assay. (C) qPCR for *Col1a1*, *Col3a1*, *Mmp2* and *Timp1* (* $p < 0.05$, ** $p < 0.01$, *** < 0.001, ANOVA, Dunn's multiple comparison test).

Figure 3: **The BCL2 antagonist decreases αSMA in murine fibroblasts.** Fibroblasts were stimulated with 5 ng/ml TGFβ, BCL2 antagonist stimulation for 24 h with the concentrations indicated. (A) Viability assay. (B) qPCR for *αSma*. (C) Western blot for αSMA, representative image for n = 3, densitometry. (D) IF, gain 900 V used for signal amplification. (E) IF of TGF-β stimulated fibroblasts, gain 600 V, 63-fold magnification, blue = DAPI, green = αSMA (* $p < 0.05$, ANOVA, Dunn's multiple comparison test).

Figure 4: **The BCL2 antagonist decreased murine fibroblast differentiation.** Fibroblasts were stimulated with 5 ng/ml TGFβ, BCL2 antagonist stimulation for 24 h with the concentrations indicated. qPCR for (A) *Col1a1* and *Col3a1*, (B) *Loxl2*, (C) *Timp1*, (D) *Tgfβ* and (E) *Il6* (* $p < 0.05$, ANOVA, Dunn's multiple comparison test).

Figure 5: **High concentrations of the BCL2 antagonist increased apoptosis in human fibroblasts.** Fibroblasts were stimulated with 5 ng/ml TGFβ, BCL2 antagonist stimulation for 24 h with the concentrations indicated. (A) Viability assay. (B) Caspase 3/7 activity. (C) IHC for cleaved caspase 3. (D) Flow cytometry (*** $p < 0.001$, ANOVA, Dunn's multiple comparison test).

Figure 6: **The BCL2 antagonist decreased αSMA in human fibroblasts.** Fibroblasts were stimulated with 5 ng/ml TGFβ, BCL2 antagonist stimulation for 24 h with the concentrations indicated. (A) qPCR for *αSMA*. (B) IF for αSMA, 63-fold magnification, blue = DAPI, green = αSMA. (C) qPCR for *COL1A1* and *COL3A1.* (D) qPCR for *TGF* (* $p < 0.05$, ANOVA, Dunn's multiple comparison test for 6A and t-test for 6C and D).

Figure 7: **The BCL2 antagonist decreased BCLXL and BCL2 in human fibroblasts.** Fibroblasts were stimulated with 5 ng/ml TGFβ, BCL2 antagonist stimulation for 24 h with the concentrations indicated. (A) Western blot for BCLXL. (B) Western blot for BCL2 (* $p < 0.05$, ** $p < 0.01$, ANOVA, Dunn's multiple comparison test).

Figure 8: **The BCL2 antagonist decreased nuclear translocation of GATA6 and pSOX9 in fibroblasts.** Fibroblasts were stimulated with 5 ng/ml TGFβ, BCL2 antagonist stimulation for 24 h with the concentrations indicated. (A) NGS cluster plot. (B) qPCR for *GATA6* and *SOX9*. (C) IF in human fibroblasts from patient 1, blue = DAPI, red = GATA6. (D) IF in murine fibroblasts, blue = DAPI, red = pSOX9. (E) IF in human fibroblasts from patient 1, blue = DAPI, red = SOX9 (63-fold magnification, * $p < 0.05$, ANOVA, Dunn's multiple comparison test).

	Gender	Age at time of fibroblast isolation (years)	Disease, intestinal segment	Disease behavior	Treatment	Date of fibroblast isolation	Date cryo-preservation	Date of renewed culture	Passage number
1	female	52	CD, colon	Mild inflammation, no fibrostenotic segment, no fistla	Azathioprine	20 Sept 2001	19 Oct 2001	Feb 2016	12-20
2	female	70	Rectum-carcinoma	No inflammation, no fibrostenotic segment	information not interrogated	02 Dec 1999	10 Feb 2000	Feb 2016	12-20

Table 1: Characteristics of patients for isolation and culture of human intestinal fibroblasts

Supplementary table: Illumina NGS using total RNA (RIN > 8.3) from primary human colonic fibroblasts from patient 1. NGS was performed by the **Functional Genomics Center Zurich. Regulation was confirmed** in two independent experimental rounds. Genes listed here were increased at least > 2-fold upon recombinant TGF-β and decreased at least > 2-fold upon additional ABT-737. Random colour code.

n-fold increase upon rTGF-β	m-fold decrease upon additional ABT-737	gene_name	description
396.6978	0.3504	TGFB2	transforming growth factor beta 2
167.1609	0.4818	TGFBI	transforming growth factor beta induced
110.0582	0.4060	ACTB	actin beta
77.8927	0.4202	ACTG1	actin gamma 1
76.1643	0.2249	COL4A3	collagen type IV alpha 3 chain
73.4180	0.3621	COL16A1	collagen type XVI alpha 1 chain
56.6342	0.3751	COL1A1	collagen type I alpha 1 chain
38.5680	0.3231	TGFB1I1	transforming growth factor beta 1 induced transcript 1
37.3079	0.3603	EMILIN2	elastin microfibril interfacer 2
36.5515	0.2195	TNFRSF11B	TNF receptor superfamily member 11b
34.6266	0.1445	ACTA2	actin, alpha 2, smooth muscle, aorta
32.6911	0.0624	ACTC1	actin, alpha, cardiac muscle 1
31.8816	0.0925	ACTG2	actin, gamma 2, smooth muscle, enteric
31.7181	0.1635	C1QTNF3	C1q and tumor necrosis factor related protein 3
31.0263	0.4431	FIBCD1	fibrinogen C domain containing 1
30.9796	0.0248	LEFTY2	left-right determination factor 2
30.9685	0.0628	MAMDC2	MAM domain containing 2
30.2886	0.1794	EDN1	endothelin 1
25.4419	0.2735	COMP	cartilage oligomeric matrix protein
23.9765	0.0574	ELN	elastin
22.6845	0.0010	NPPB	natriuretic peptide B
21.8715	0.0051	CYP24A1	cytochrome P450 family 24 subfamily A member 1
21.2773	0.0169	IGF1	insulin like growth factor 1
21.0261	0.0221	PLN	phospholamban
20.8501	0.0229	NOTUM	NOTUM, palmitoleoyl-protein carboxylesterase
20.5072	0.0262	KRT80	keratin 80

20.2989	0.0267	ASB2	ankyrin repeat and SOCS box containing 2
20.2166	0.0297	EXTL1	exostosin like glycosyltransferase 1
20.1477	0.0333	METTL21C	methyltransferase like 21C
20.0597	0.0338	AMDHD1	amidohydrolase domain containing 1
19.3253	0.0385		ABC7-42404400C24.1
19.3124	0.0429	NXPH3	neurexophilin 3
19.2814	0.0439	HBD	hemoglobin subunit delta
19.2655	0.0443	KRT86	keratin 86
18.3833	0.0473	TAS2R31	taste 2 receptor member 31
18.2893	0.0525	ASB9	ankyrin repeat and SOCS box containing 9
18.1638	0.0545	RP11-136C24.3	
17.3237	0.0590	GBP1	guanylate binding protein 1
17.0576	0.0638	CXCL10	C-X-C motif chemokine ligand 10
17.0468	0.0645	CAPN6	calpain 6
16.8788	0.0654	MECOM	MDS1 and EVI1 complex locus
16.7453	0.0864	SFRP4	secreted frizzled related protein 4
16.0284	0.0898	SYT12	synaptotagmin 12
15.4935	0.0915	KRBOX1	KRAB box domain containing 1
15.2777	0.0958	KCNMB1	potassium calcium-activated channel subfamily M regulatory beta subunit 1
14.7023	0.0975	PPP1R14A	protein phosphatase 1 regulatory inhibitor subunit 14A
14.6936	0.1027	MUM1L1	MUM1 like 1
14.4584	0.1103	GATM	glycine amidinotransferase
13.9967	0.1113	FAM150A	family with sequence similarity 150 member A
13.6053	0.1132	PCSK1N	proprotein convertase subtilisin/kexin type 1 inhibitor
13.1272	0.1162	SERTAD4	SERTA domain containing 4
13.0214	0.1182	MYLK2	myosin light chain kinase 2
12.8480	0.1182	CNN1	calponin 1
12.7848	0.1184	LDB3	LIM domain binding 3
12.6418	0.1184	RASL12	RAS like family 12
12.3655	0.1200	MEGF6	multiple EGF like domains 6
12.2294	0.1203	HSD17B6	hydroxysteroid 17-beta dehydrogenase 6
11.9969	0.1240	DPT	dermatopontin
11.7727	0.1285	LRRN3	leucine rich repeat neuronal 3
11.6885	0.1347	SCN7A	sodium voltage-gated channel alpha subunit 7

11.6652	0.1375	HSPB1	heat shock protein family B (small) member 1
11.4853	0.1389	PLEKHA7	pleckstrin homology domain containing A7
11.3302	0.1428	MYH11	myosin heavy chain 11
11.2719	0.1466	CRISPLD2	cysteine rich secretory protein LCCL domain containing 2
11.1907	0.1467	CSDC2	cold shock domain containing C2
11.1419	0.1512	DKK2	dickkopf WNT signaling pathway inhibitor 2
10.8727	0.1529	LHFPL1	lipoma HMGIC fusion partner-like 1
10.7677	0.1575	LBP	lipopolysaccharide binding protein
10.5703	0.1589	DUSP26	dual specificity phosphatase 26 (putative)
10.5631	0.1599	KRT18	keratin 18
10.5593	0.1605	KRT7	keratin 7
10.5207	0.1666	KANK4	KN motif and ankyrin repeat domains 4
10.4254	0.1691	WISP1	WNT1 inducible signaling pathway protein 1
10.4119	0.1693	LIMS2	LIM zinc finger domain containing 2
10.3276	0.1695	RASGRP3	RAS guanyl releasing protein 3
10.2991	0.1703	INMT	indolethylamine N-methyltransferase
10.2087	0.1704	SULT1A3	sulfotransferase family 1A member 3
10.1196	0.1721	F3	coagulation factor III, tissue factor
10.1087	0.1764	ID1	inhibitor of DNA binding 1, HLH protein
9.9288	0.1805	GLI1	GLI family zinc finger 1
9.8984	0.1812	SYT16	synaptotagmin 16
9.8119	0.1819	HIST1H3A	histone cluster 1 H3 family member a
9.7494	0.1824	LMNB1	lamin B1
9.7319	0.1833	CNN2	calponin 2
9.5970	0.1864	PRL	prolactin
9.5815	0.1876	PTGES3L	prostaglandin E synthase 3 like
9.4995	0.1918	OXTR	oxytocin receptor
9.3506	0.1919	RASGRP1	RAS guanyl releasing protein 1
9.3334	0.1924	SYCP2L	synaptonemal complex protein 2 like
9.3129	0.1933	PLA2G2A	phospholipase A2 group IIA
9.1356	0.2039	ANO4	anoctamin 4
9.1004	0.2083	ARHGDIB	Rho GDP dissociation inhibitor beta
9.0399	0.2107	GLIPR2	GLI pathogenesis related 2
8.9303	0.2117	CD200	CD200 molecule

8.9037	0.2120	CDKN2B	cyclin dependent kinase inhibitor 2B
8.8893	0.2183	RHBDL2	rhomboid like 2
8.8060	0.2244	TET1	tet methylcytosine dioxygenase 1
8.5031	0.2247	KCNN4	potassium calcium-activated channel subfamily N member 4
8.4446	0.2302	BDNF	brain derived neurotrophic factor
8.4278	0.2341	CRABP2	cellular retinoic acid binding protein 2
8.4207	0.2376	CILP	cartilage intermediate layer protein
8.2698	0.2387	CCL11	C-C motif chemokine ligand 11
8.2284	0.2416	WTH3DI	RAB6C-like
8.1777	0.2426	CLIC3	chloride intracellular channel 3
8.1738	0.2431	OPCML	opioid binding protein/cell adhesion molecule like
8.1635	0.2432	LGALS9	galectin 9
8.1224	0.2436	UMODL1	uromodulin like 1
8.0546	0.2457	CALB2	calbindin 2
7.8920	0.2466	RASL11B	RAS like family 11 member B
7.8590	0.2485	PRRX2	paired related homeobox 2
7.7749	0.2486	CORO2A	coronin 2A
7.7584	0.2523	NOX4	NADPH oxidase 4
7.7154	0.2555	RASSF2	Ras association domain family member 2
7.7011	0.2566	NTRK2	neurotrophic receptor tyrosine kinase 2
7.6615	0.2579	EGLN3	egl-9 family hypoxia inducible factor 3
7.6200	0.2585	CDA	cytidine deaminase
7.6102	0.2592	RSPH4A	radial spoke head 4 homolog A
7.5703	0.2606	CSRP2	cysteine and glycine rich protein 2
7.5008	0.2660	OLFM2	olfactomedin 2
7.3854	0.2675	FGF9	fibroblast growth factor 9
7.3710	0.2702	XG	Xg blood group
7.3529	0.2728	RAPGEF4	Rap guanine nucleotide exchange factor 4
7.3050	0.2759	TSPAN2	tetraspanin 2
7.2458	0.2765	OLFML2B	olfactomedin like 2B
7.1969	0.2788	LMTK3	lemur tyrosine kinase 3
7.1058	0.2838	TREH	trehalase
7.0696	0.2868	JPH2	junctophilin 2
7.0614	0.2874	MYADM	myeloid associated differentiation marker

7.0065	0.2874	BIRC7	baculoviral IAP repeat containing 7
7.0054	0.2938	ATRNL1	attractin like 1
6.8786	0.3016	LUZP2	leucine zipper protein 2
6.8630	0.3046	SLX1A	SLX1 homolog A, structure-specific endonuclease subunit
6.8359	0.3076	SAMD11	sterile alpha motif domain containing 11
6.8093	0.3104	ITGB1BP2	integrin subunit beta 1 binding protein 2
6.7261	0.3116	WFDC1	WAP four-disulfide core domain 1
6.7149	0.3190	EPHA3	EPH receptor A3
6.7028	0.3199	EPB41L4B	erythrocyte membrane protein band 4.1 like 4B
6.6794	0.3228	LRRC17	leucine rich repeat containing 17
6.6539	0.3276	UHRF1	ubiquitin like with PHD and ring finger domains 1
6.6508	0.3307	KSR1	kinase suppressor of ras 1
6.6373	0.3338	FAM181B	family with sequence similarity 181 member B
6.6078	0.3342	RP11-849H4.2	Putative short transient receptor potential channel 2-like protein
6.5624	0.3393	ADAM19	ADAM metallopeptidase domain 19
6.4773	0.3399	GSTT2B	glutathione S-transferase theta 2B (gene/pseudogene)
6.4297	0.3417	JADE1	jade family PHD finger 1
6.3525	0.3430	HOPX	HOP homeobox
6.2709	0.3437	WISP2	WNT1 inducible signaling pathway protein 2
6.2553	0.3463	SRRM3	serine/arginine repetitive matrix 3
6.2325	0.3485	IL17B	interleukin 17B
6.1909	0.3505	OLR1	oxidized low density lipoprotein receptor 1
6.1805	0.3505	OR2B6	olfactory receptor family 2 subfamily B member 6
6.1628	0.3544	TRIL	TLR4 interactor with leucine rich repeats
6.1593	0.3556	SYT3	synaptotagmin 3
6.1558	0.3567	TAC3	tachykinin 3
6.1316	0.3570	FST	follistatin
6.0911	0.3583	FSCN2	fascin actin-bundling protein 2, retinal
6.0507	0.3585	NUAK2	NUAK family kinase 2
6.0502	0.3603	MEX3A	mex-3 RNA binding family member A
6.0359	0.3631	HEYL	hes related family bHLH transcription factor with YRPW motif-like
5.9151	0.3639	LMCD1	LIM and cysteine rich domains 1
5.9095	0.3658	HIST1H2BO	histone cluster 1 H2B family member o
5.8627	0.3676	FAM19A5	family with sequence similarity 19 member A5, C-C motif chemokine like

5.8573	0.3689	NREP	neuronal regeneration related protein
5.8419	0.3713	AC015688.3	
5.8293	0.3727	CALD1	caldesmon 1
5.8269	0.3731	ASPN	asporin
5.7969	0.3749	CLSTN2	calsyntenin 2
5.6873	0.3779	PRPS1	phosphoribosyl pyrophosphate synthetase 1
5.6776	0.3786	WNT11	Wnt family member 11
5.6623	0.3791	CDH6	cadherin 6
5.6583	0.3820	PALLD	palladin, cytoskeletal associated protein
5.6183	0.3847	C16orf87	chromosome 16 open reading frame 87
5.6141	0.3848	TPM1	tropomyosin 1 (alpha)
5.6094	0.3861	XAF1	XIAP associated factor 1
5.6051	0.3870	SGK223	Tyrosine-protein kinase SgK223
5.5269	0.3874	GATA6	GATA binding protein 6
5.5062	0.3891	TAGLN	transgelin
5.5002	0.3901	FAM133A	family with sequence similarity 133 member A
5.4844	0.3915	LOXL1	lysyl oxidase like 1
5.4618	0.3918	C12orf73	chromosome 12 open reading frame 73
5.3986	0.3939	ESCO2	establishment of sister chromatid cohesion N-acetyltransferase 2
5.3871	0.3996	DZIP1L	DAZ interacting zinc finger protein 1 like
5.3801	0.3997	NLRP1	NLR family pyrin domain containing 1
5.3797	0.4026	ALOX5AP	arachidonate 5-lipoxygenase activating protein
5.3415	0.4060	FSCN1	fascin actin-bundling protein 1
5.3364	0.4073	AQP1	aquaporin 1 (Colton blood group)
5.3042	0.4105	ZCCHC18	zinc finger CCHC-type containing 18
5.2945	0.4171	EFNB2	ephrin B2
5.2788	0.4176	MISP	mitotic spindle positioning
5.2776	0.4212	TC2N	tandem C2 domains, nuclear
5.2605	0.4230	NOG	noggin
5.2452	0.4246	TMEM92	transmembrane protein 92
5.1804	0.4249	SLC38A5	solute carrier family 38 member 5
5.1782	0.4249	ETV6	ETS variant 6
5.1782	0.4253	CALY	calcyon neuron specific vesicular protein
5.1530	0.4260	PDLIM7	PDZ and LIM domain 7

5.0934	0.4266	KCNH1	potassium voltage-gated channel subfamily H member 1
5.0717	0.4269	SRF	serum response factor
5.0677	0.4284	NTS	neurotensin
5.0661	0.4291	PPME1	protein phosphatase methylesterase 1
5.0569	0.4326	RFPL4A	ret finger protein like 4A
5.0568	0.4327	TTC9	tetratricopeptide repeat domain 9
5.0457	0.4339	IVNS1ABP	influenza virus NS1A binding protein
5.0371	0.4342	BGN	biglycan
5.0035	0.4374	PECAM1	platelet and endothelial cell adhesion molecule 1
4.9848	0.4386	C9orf3	chromosome 9 open reading frame 3
4.9806	0.4395	NEFH	neurofilament heavy polypeptide
4.9805	0.4445	MARCKSL1	MARCKS like 1
4.9538	0.4457	RASD2	RASD family member 2
4.9327	0.4458	TGM1	transglutaminase 1
4.9062	0.4474	CST1	cystatin SN
4.8994	0.4489	HABP2	hyaluronan binding protein 2
4.8822	0.4507	SORBS2	sorbin and SH3 domain containing 2
4.8760	0.4513	LIMK2	LIM domain kinase 2
4.8744	0.4527	NOTCH3	notch 3
4.8708	0.4621	SGCA	sarcoglycan alpha
4.8686	0.4627	TYRP1	tyrosinase related protein 1
4.8677	0.4631	USP43	ubiquitin specific peptidase 43
4.8498	0.4633	UCP3	uncoupling protein 3
4.8466	0.4646	UACA	uveal autoantigen with coiled-coil domains and ankyrin repeats
4.8404	0.4663	DIO2	deiodinase, iodothyronine type II
4.8016	0.4666	NKD1	naked cuticle homolog 1
4.7891	0.4669	KCTD16	potassium channel tetramerization domain containing 16
4.7672	0.4689	PDE4C	phosphodiesterase 4C
4.7521	0.4693	SORBS1	sorbin and SH3 domain containing 1
4.7417	0.4706	DNAJB5	DnaJ heat shock protein family (Hsp40) member B5
4.7194	0.4719	STK38L	serine/threonine kinase 38 like
4.6980	0.4724	ZCCHC12	zinc finger CCHC-type containing 12
4.6792	0.4725	APOL4	apolipoprotein L4
4.6704	0.4728	LRRC4B	leucine rich repeat containing 4B

4.6658	0.4737	FRMPD3	FERM and PDZ domain containing 3
4.6592	0.4746	OPN3	opsin 3
4.6482	0.4749	LANCL2	LanC like 2
4.6444	0.4769	MAP3K7CL	MAP3K7 C-terminal like
4.6321	0.4792	KLC3	kinesin light chain 3
4.6199	0.4810	SOX9	SRY-box 9
4.6170	0.4813	DDAH1	dimethylarginine dimethylaminohydrolase 1
4.6140	0.4841	THBS1	thrombospondin 1
4.5972	0.4842	NPR3	natriuretic peptide receptor 3
4.5952	0.4848	PRG4	proteoglycan 4
4.5767	0.4858	ZNF93	zinc finger protein 93
4.5607	0.4878	ALDH1B1	aldehyde dehydrogenase 1 family member B1
4.5513	0.4918	CGB7	chorionic gonadotropin beta subunit 7
4.5416	0.4972	FGF1	fibroblast growth factor 1
4.5288	0.4973	SMCO2	single-pass membrane protein with coiled-coil domains 2
4.5046	0.4974	IL21R	interleukin 21 receptor
4.4939	0.4997	TXNDC5	thioredoxin domain containing 5

relevant genes missing the > 2-fold requirement

2.9998	*0.5907*	*ACTA1*	*actin, alpha 1, skeletal muscle*
2.9060	*0.6459*	*TGFBR1*	*transforming growth factor beta receptor 1*
2.1811	*1.4010*	*TGFB1*	*transforming growth factor beta 1*

Figure 1

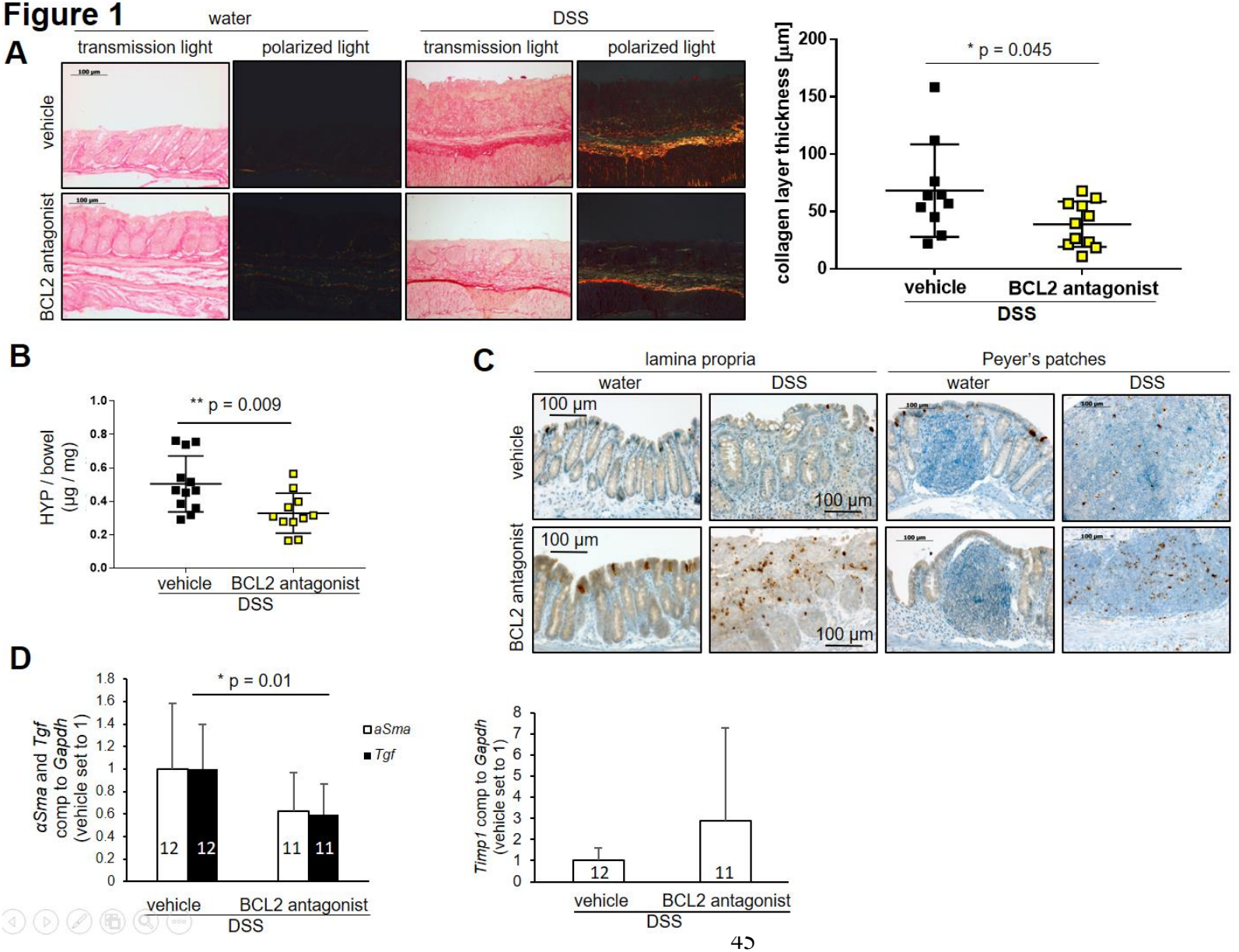
A
water
DSS
transmission light
polarized light
transmission light
polarized light
vehicle
BCL2 antagonist
100 µm
collagen layer thickness [µm]
200
150
100
50
0
* p = 0.045
vehicle
BCL2 antagonist
DSS
B
** p = 0.009
HYP / bowel (µg / mg)
1.0
0.8
0.6
0.4
0.2
0.0
vehicle
BCL2 antagonist
DSS
C
lamina propria
Peyer's patches
water
DSS
water
DSS
vehicle
BCL2 antagonist
100 µm
D
* p = 0.01
αSma and Tgf comp to Gapdh (vehicle set to 1)
aSma
Tgf
12
12
11
11
vehicle
BCL2 antagonist
DSS
Timp1 comp to Gapdh (vehicle set to 1)
12
11
vehicle
BCL2 antagonist
DSS

Figure 2

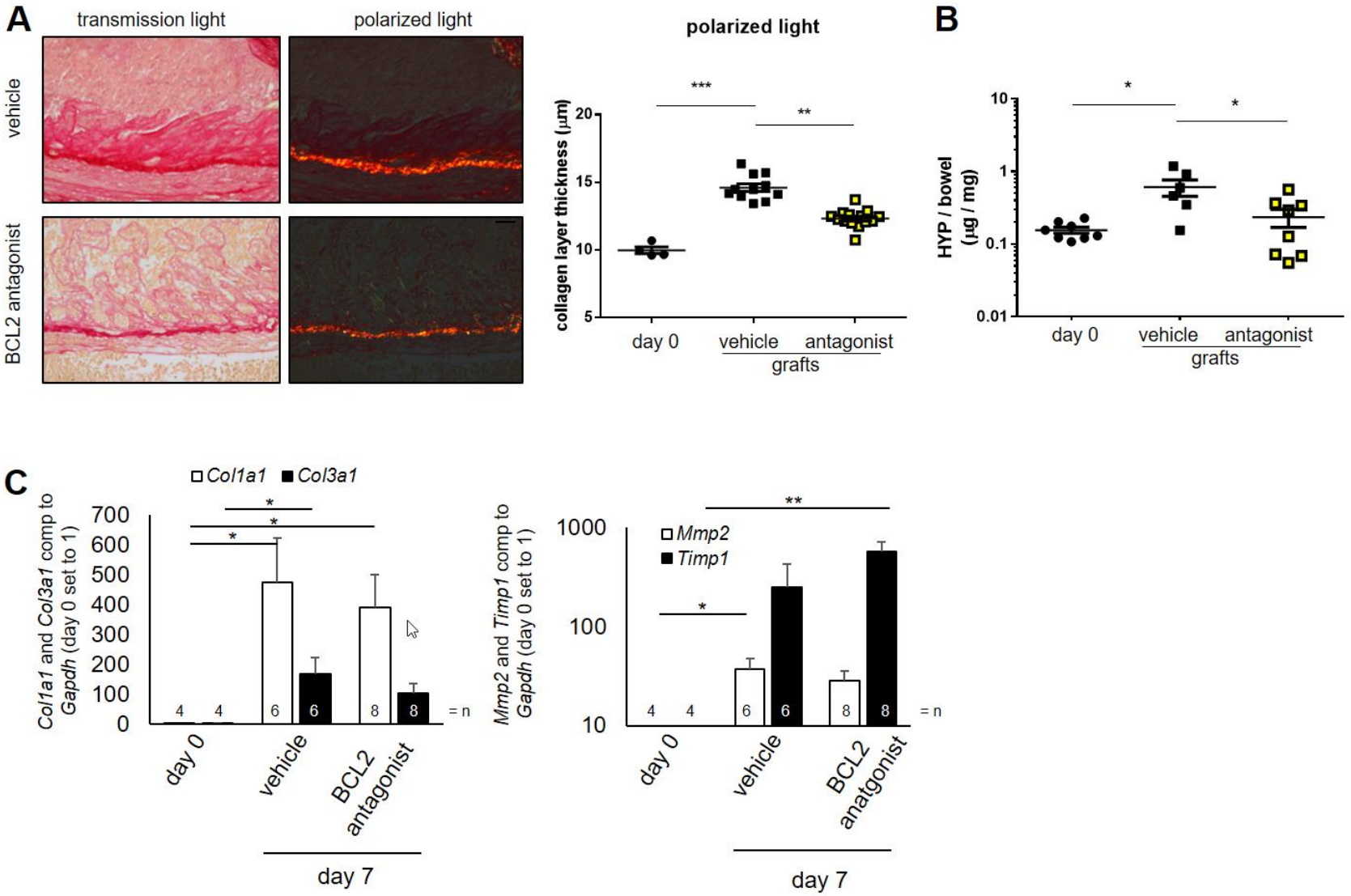
A
transmission light
polarized light
vehicle
BCL2 antagonist
polarized light
collagen layer thickness (µm)
day 0
vehicle
antagonist
grafts
B
HYP / bowel (µg / mg)
day 0
vehicle
antagonist
grafts
C
Col1a1
Col3a1
Col1a1 and Col3a1 comp to Gapdh (day 0 set to 1)
day 0
vehicle
BCL2 antagonist
day 7
Mmp2
Timp1
Mmp2 and Timp1 comp to Gapdh (day 0 set to 1)
BCL2 anatgonist

Figure 3

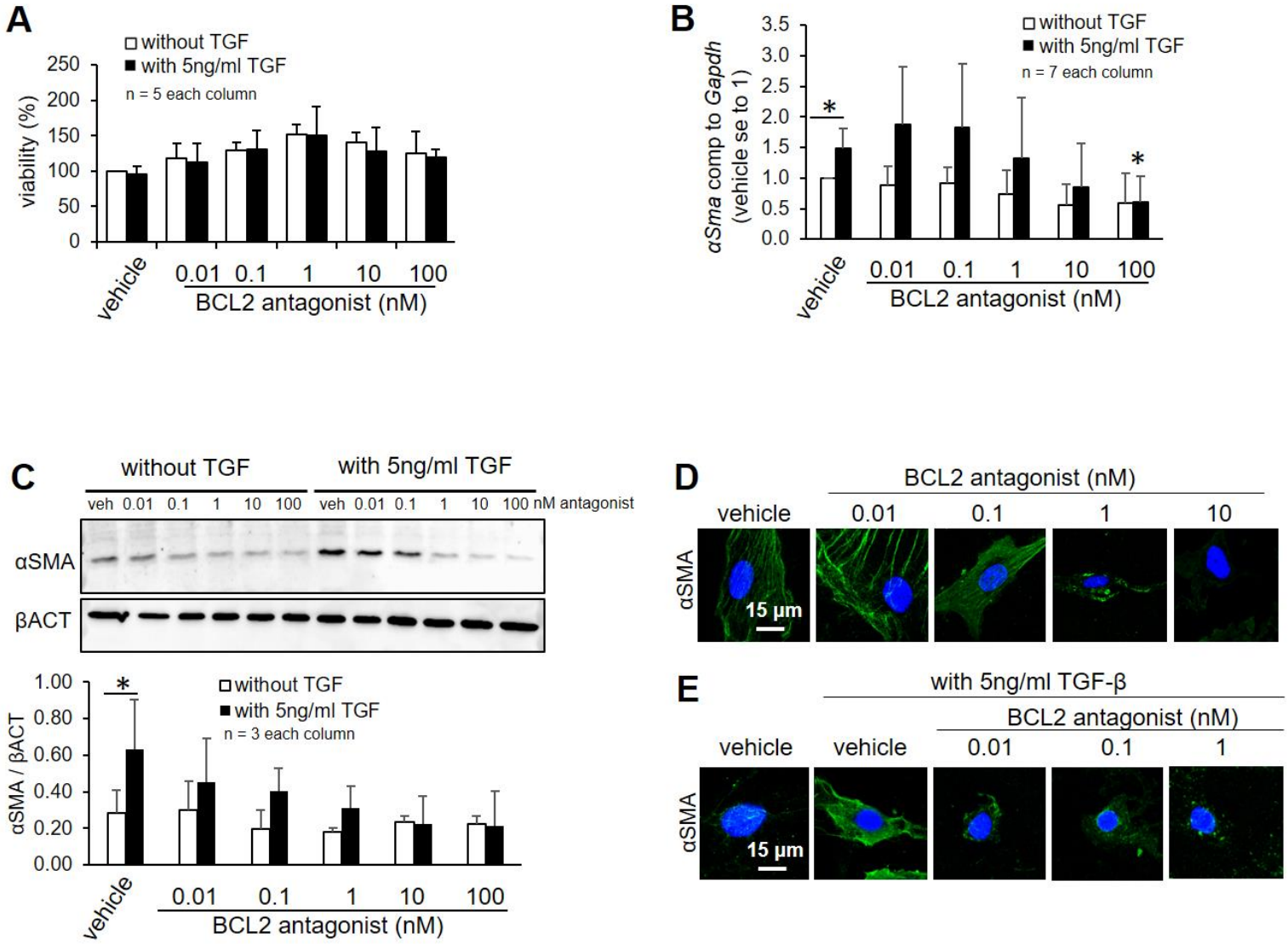
A
without TGF
with 5ng/ml TGF
n = 5 each column
viability (%)
250
200
150
100
50
0
vehicle
0.01 0.1 1 10 100
BCL2 antagonist (nM)
B
without TGF
with 5ng/ml TGF
n = 7 each column
αSma comp to Gapdh (vehicle se to 1)
3.5
3.0
2.5
2.0
1.5
1.0
0.5
0.0
*
*
vehicle
0.01 0.1 1 10 100
BCL2 antagonist (nM)
C
without TGF
with 5ng/ml TGF
veh 0.01 0.1 1 10 100 veh 0.01 0.1 1 10 100 nM antagonist
αSMA
βACT
without TGF
with 5ng/ml TGF
n = 3 each column
αSMA / βACT
1.00
0.80
0.60
0.40
0.20
0.00
*
vehicle
0.01 0.1 1 10 100
BCL2 antagonist (nM)
D
BCL2 antagonist (nM)
vehicle
0.01
0.1
1
10
αSMA
15 µm
E
with 5ng/ml TGF-β
BCL2 antagonist (nM)
vehicle
vehicle
0.01
0.1
1
αSMA
15 µm

Figure 4

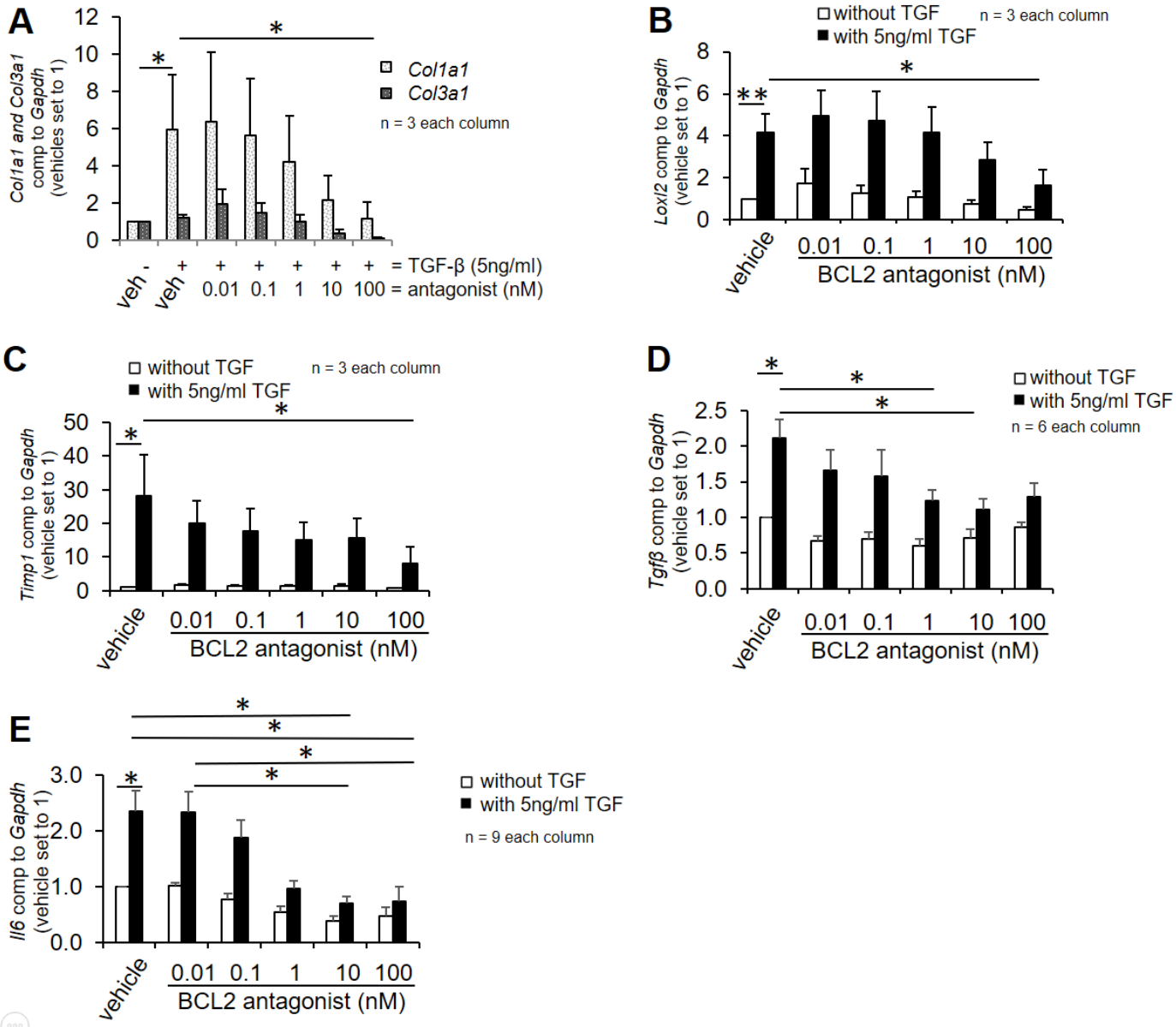
A
Col1a1 and Col3a1 comp to Gapdh (vehicles set to 1)
Col1a1
Col3a1
n = 3 each column
veh - veh + 0.01 0.1 1 10 100 = TGF-β (5ng/ml)
= antagonist (nM)
B
without TGF
with 5ng/ml TGF
n = 3 each column
Loxl2 comp to Gapdh (vehicle set to 1)
vehicle 0.01 0.1 1 10 100
BCL2 antagonist (nM)
C
without TGF
with 5ng/ml TGF
n = 3 each column
Timp1 comp to Gapdh (vehicle set to 1)
vehicle 0.01 0.1 1 10 100
BCL2 antagonist (nM)
D
without TGF
with 5ng/ml TGF
n = 6 each column
Tgfβ comp to Gapdh (vehicle set to 1)
vehicle 0.01 0.1 1 10 100
BCL2 antagonist (nM)
E
without TGF
with 5ng/ml TGF
n = 9 each column
Il6 comp to Gapdh (vehicle set to 1)
vehicle 0.01 0.1 1 10 100
BCL2 antagonist (nM)

Figure 5

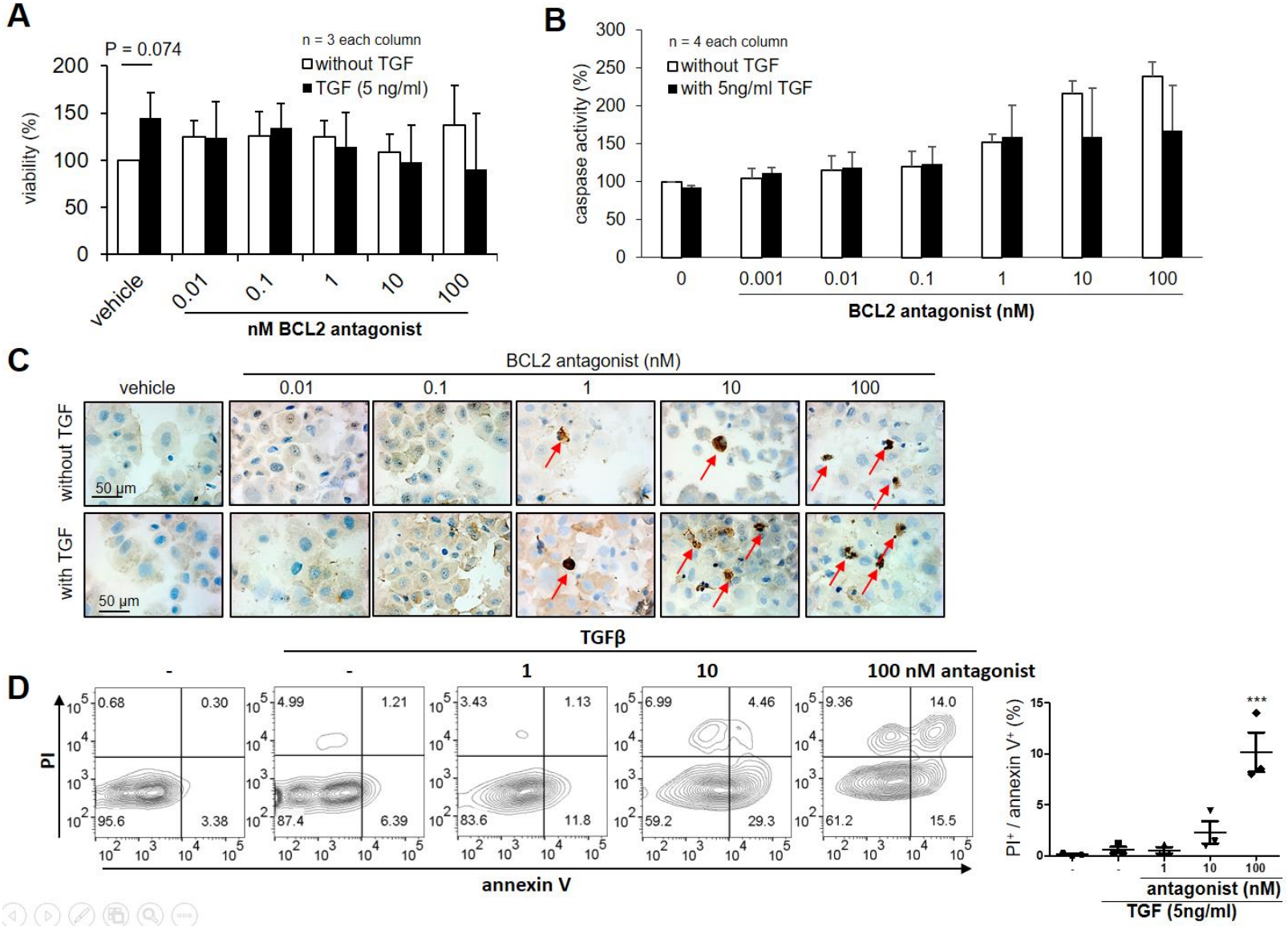
A
P = 0.074
n = 3 each column
without TGF
TGF (5 ng/ml)
viability (%)
200
150
100
50
0
vehicle
0.01
0.1
1
10
100
nM BCL2 antagonist
B
n = 4 each column
without TGF
with 5ng/ml TGF
caspase activity (%)
300
250
200
150
100
50
0
0
0.001
0.01
0.1
1
10
100
BCL2 antagonist (nM)
C
BCL2 antagonist (nM)
vehicle
0.01
0.1
1
10
100
without TGF
with TGF
50 µm
50 µm
TGFβ
D
-
-
1
10
100 nM antagonist
PI
annexin V
0.68
0.30
95.6
3.38
4.99
1.21
87.4
6.39
3.43
1.13
83.6
11.8
6.99
4.46
59.2
29.3
9.36
14.0
61.2
15.5
PI⁺ / annexin V⁺ (%)
15
10
5
0
***
-
-
1
10
100
antagonist (nM)
TGF (5ng/ml)

Figure 6

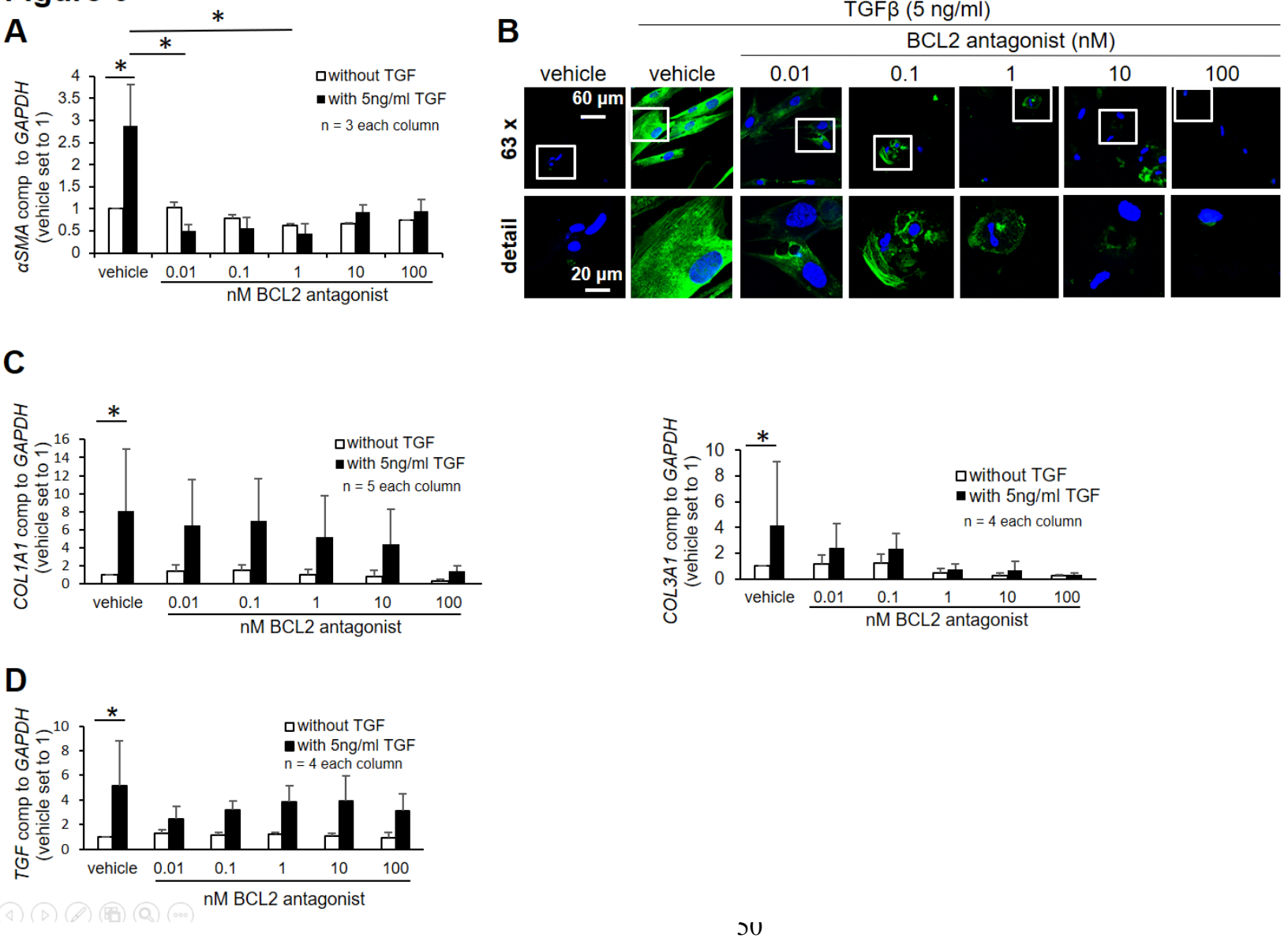
A
αSMA comp to GAPDH (vehicle set to 1)
without TGF
with 5ng/ml TGF
n = 3 each column
vehicle
0.01
0.1
1
10
100
nM BCL2 antagonist
B
TGFβ (5 ng/ml)
BCL2 antagonist (nM)
vehicle
vehicle
0.01
0.1
1
10
100
63 x
detail
60 µm
20 µm
C
COL1A1 comp to GAPDH (vehicle set to 1)
without TGF
with 5ng/ml TGF
n = 5 each column
nM BCL2 antagonist
COL3A1 comp to GAPDH (vehicle set to 1)
without TGF
with 5ng/ml TGF
n = 4 each column
nM BCL2 antagonist
D
TGF comp to GAPDH (vehicle set to 1)
without TGF
with 5ng/ml TGF
n = 4 each column
nM BCL2 antagonist

Figure 7 A

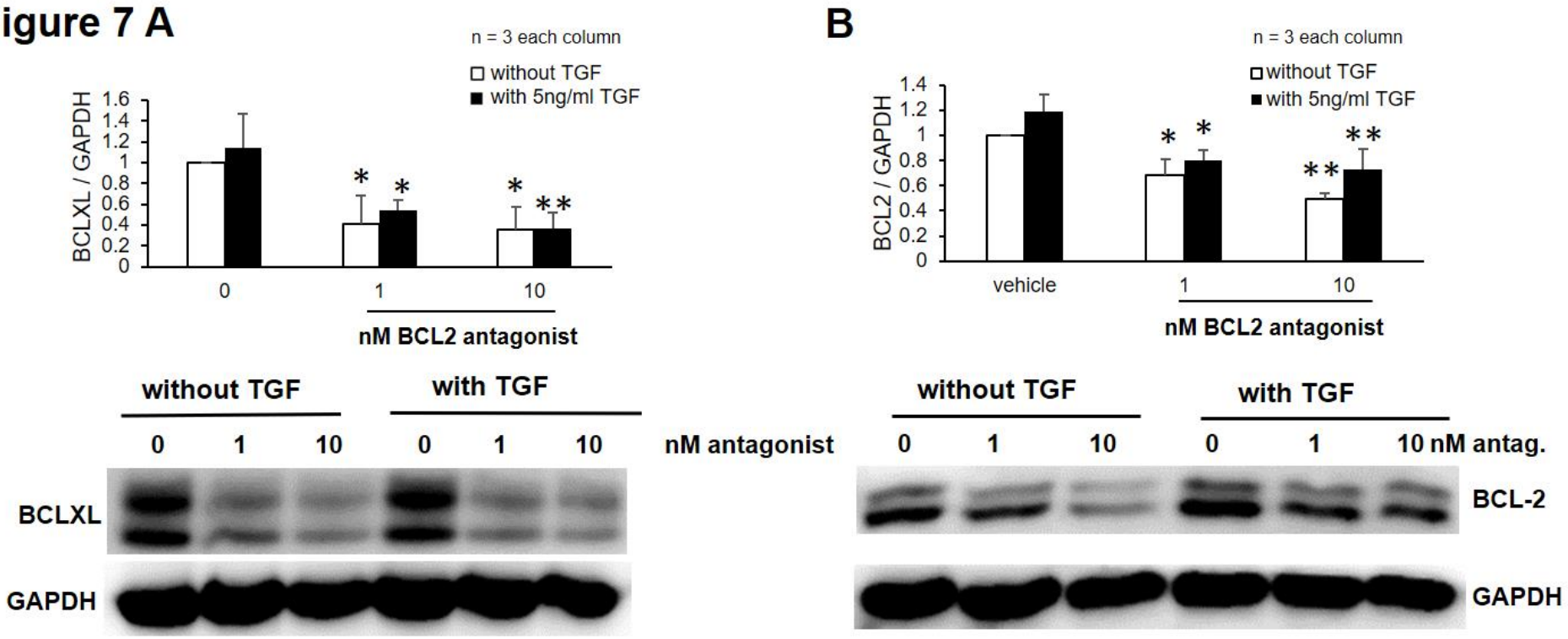
n = 3 each column
without TGF
with 5ng/ml TGF
BCLXL / GAPDH
1.6
1.4
1.2
1
0.8
0.6
0.4
0.2
0
0
1
10
nM BCL2 antagonist
without TGF
with TGF
0
1
10
0
1
10
nM antagonist
BCLXL
GAPDH
B
n = 3 each column
without TGF
with 5ng/ml TGF
BCL2 / GAPDH
1.4
1.2
1
0.8
0.6
0.4
0.2
0
vehicle
1
10
nM BCL2 antagonist
without TGF
with TGF
0
1
10
0
1
10 nM antag.
BCL-2
GAPDH

Figure 8

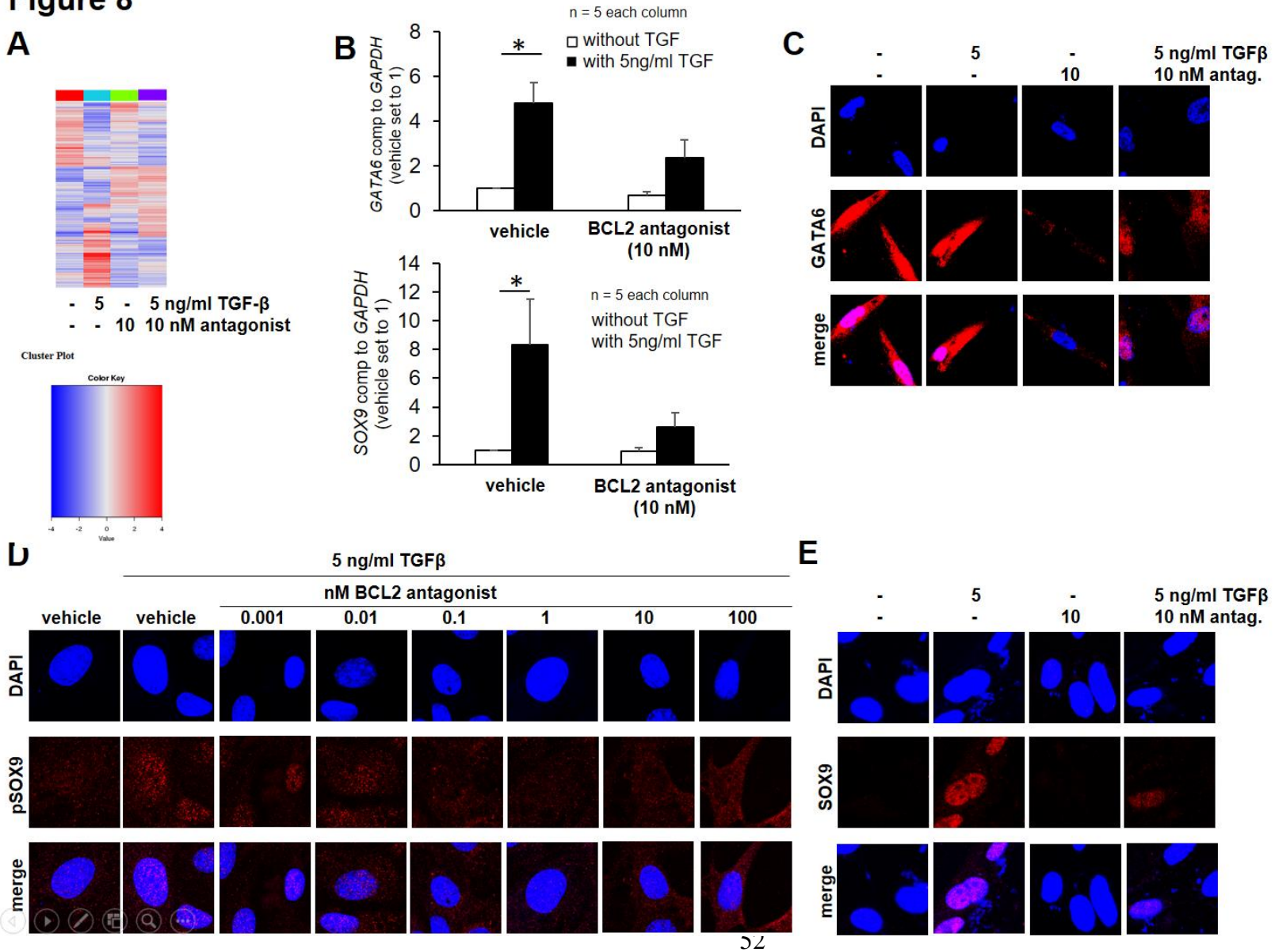
A
- 5 - 5 ng/ml TGF-β
- - 10 10 nM antagonist
Cluster Plot
Color Key
Value
B
n = 5 each column
without TGF
with 5ng/ml TGF
GATA6 comp to GAPDH (vehicle set to 1)
vehicle
BCL2 antagonist (10 nM)
SOX9 comp to GAPDH (vehicle set to 1)
n = 5 each column
without TGF
with 5ng/ml TGF
vehicle
BCL2 antagonist (10 nM)
C
- 5 - 5 ng/ml TGFβ
- - 10 10 nM antag.
DAPI
GATA6
merge
D
5 ng/ml TGFβ
nM BCL2 antagonist
vehicle vehicle 0.001 0.01 0.1 1 10 100
DAPI
pSOX9
merge
E
- 5 - 5 ng/ml TGFβ
- - 10 10 nM antag.
DAPI
SOX9
merge

Supplementary figure 1

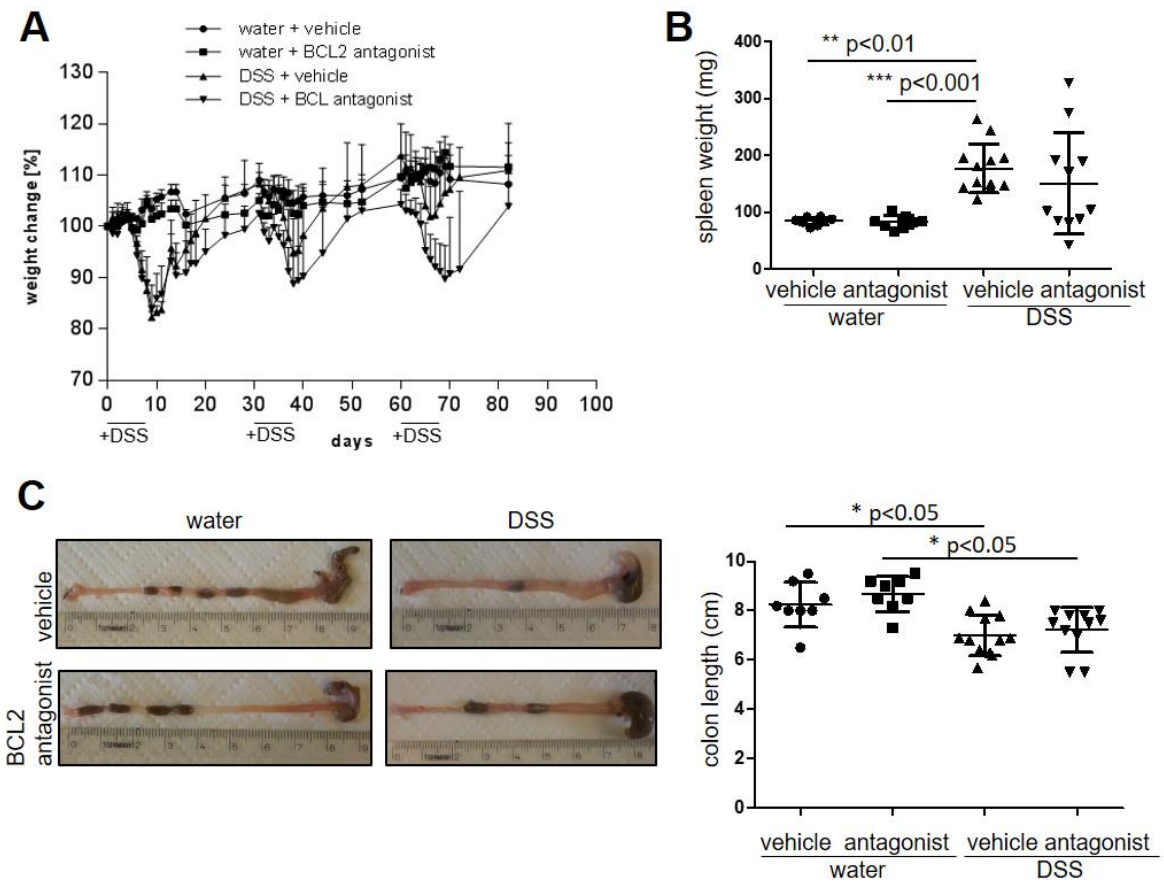

Supplementary figure 1: **Successful induction of chronic colitis.** (A) During DSS-application weight loss of BCL2 antagonist-treated mice was higher compared to vehicle but all mice gained body weight at the same level during 14 day periods of recovery.
(B) Spleen weight was increased in DSS-induced chronic colitis upon vehicle compared to BCL2 antagonist treated mice. (C) Colon length was significantly decreased following DSS-application. ANOVA, Dunn's multiple comparison test. Mean value und standard deviation are shown.

Supplementary figure 2

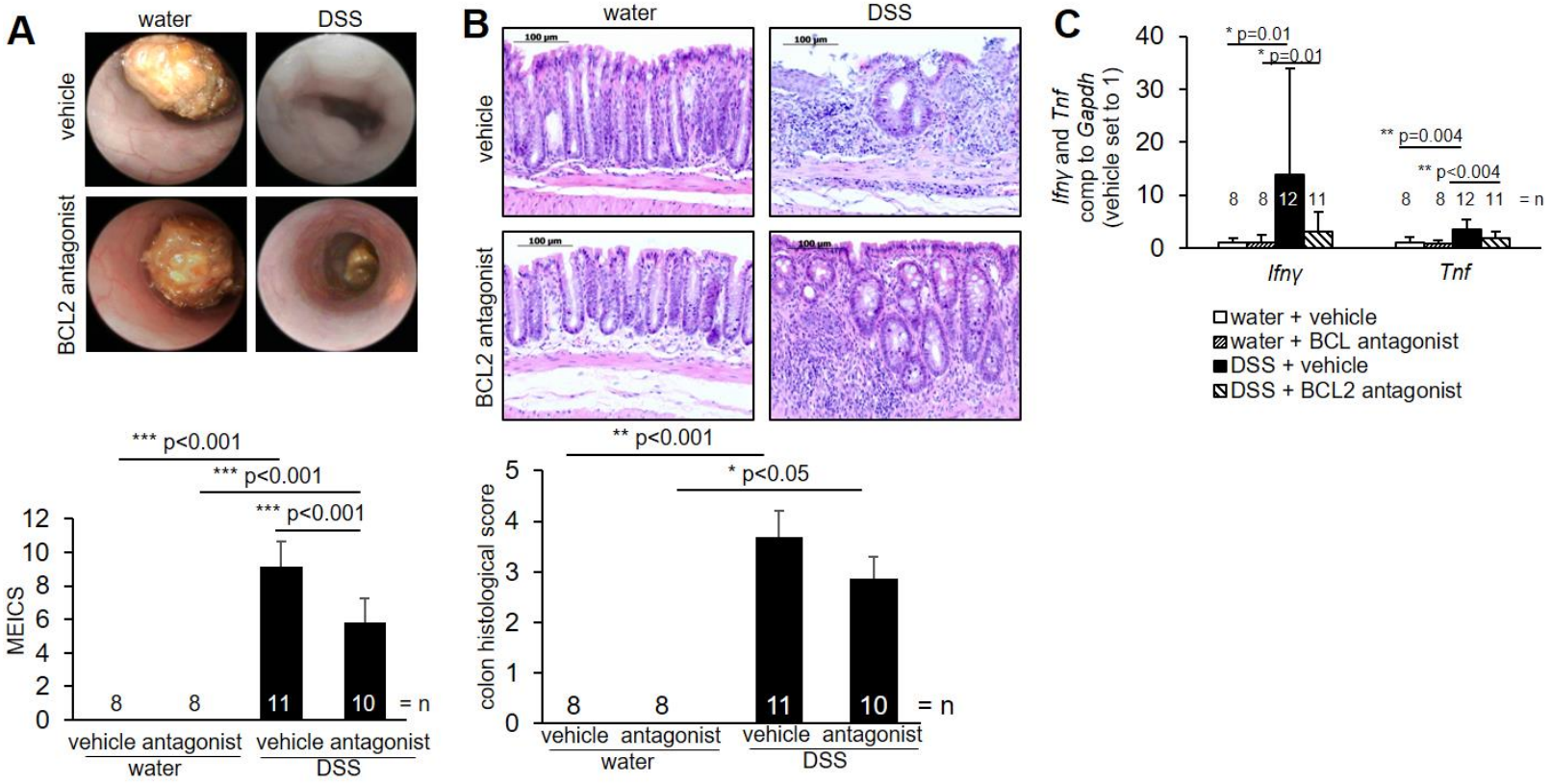

Supplementary figure 2: **Decreased inflammation upon BCL2 antagonist in DSS-induced chronic colitis.** (A) The macroscopic mucosal damage was assessed by colonoscopy and MEICS. Mucosa from mice without DSS-induced colitis displayed a smooth and transparent mucosa with a normal vascular pattern and a solid stool. After induction of colitis the colon of vehicle-treated mice appeared with a thickened and more granular mucosa without stool compared to BCL2 antagonist-treated mice with a clear vascular pattern, improved transparency and loose stool. Vehicle-treated animals exhibited significantly higher MEICS score compared to BCL2 antagonist-treated mice.
(B) H&E staining and histological score. Following DSS-induced chronic colitis histological score revealed a more severe colitis in vehicle-treated mice compared to BCL2 antagonist-treated mice.
(C) qPCR for *Ifnγ* and *Tnf*. ANOVA, Dunn's multiple comparison test. Mean value und standard deviation are shown.

Supplementary figure 3

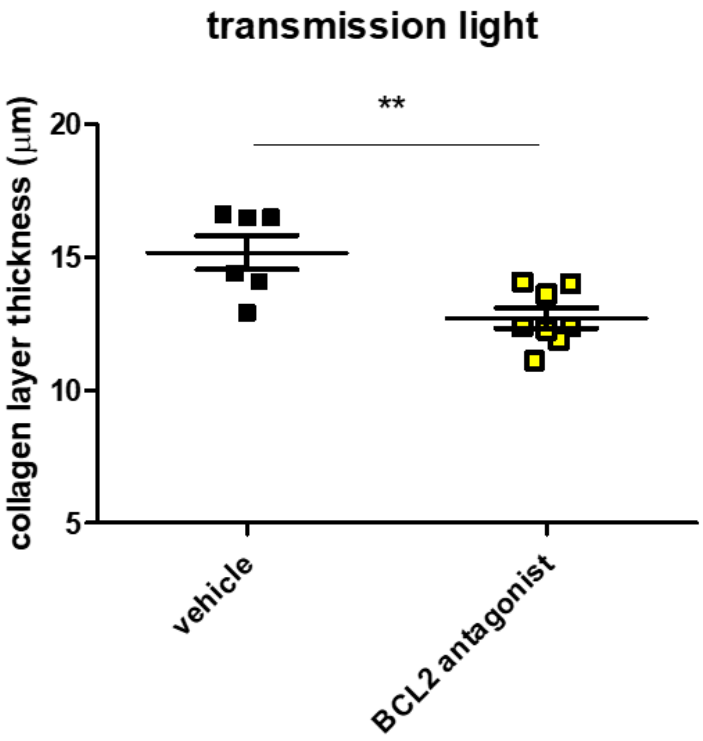

Supplementary figure 3: **Collagen layer thickness is significantly decreased following administration of BCL2 antagonist in grafts from the heterotopic transplantation model.** Sirius Red staining. Transmission light showed significantly decreased collagen layer thickness upon treatment with the BCL2 antagonist compared to vehicle (** $p < 0.01$). n as indicated. Thickness was calculated from at least eight places in representative areas at 10-fold magnification for each single graft. Mean value und standard deviation are shown.

Supplementary figure 4

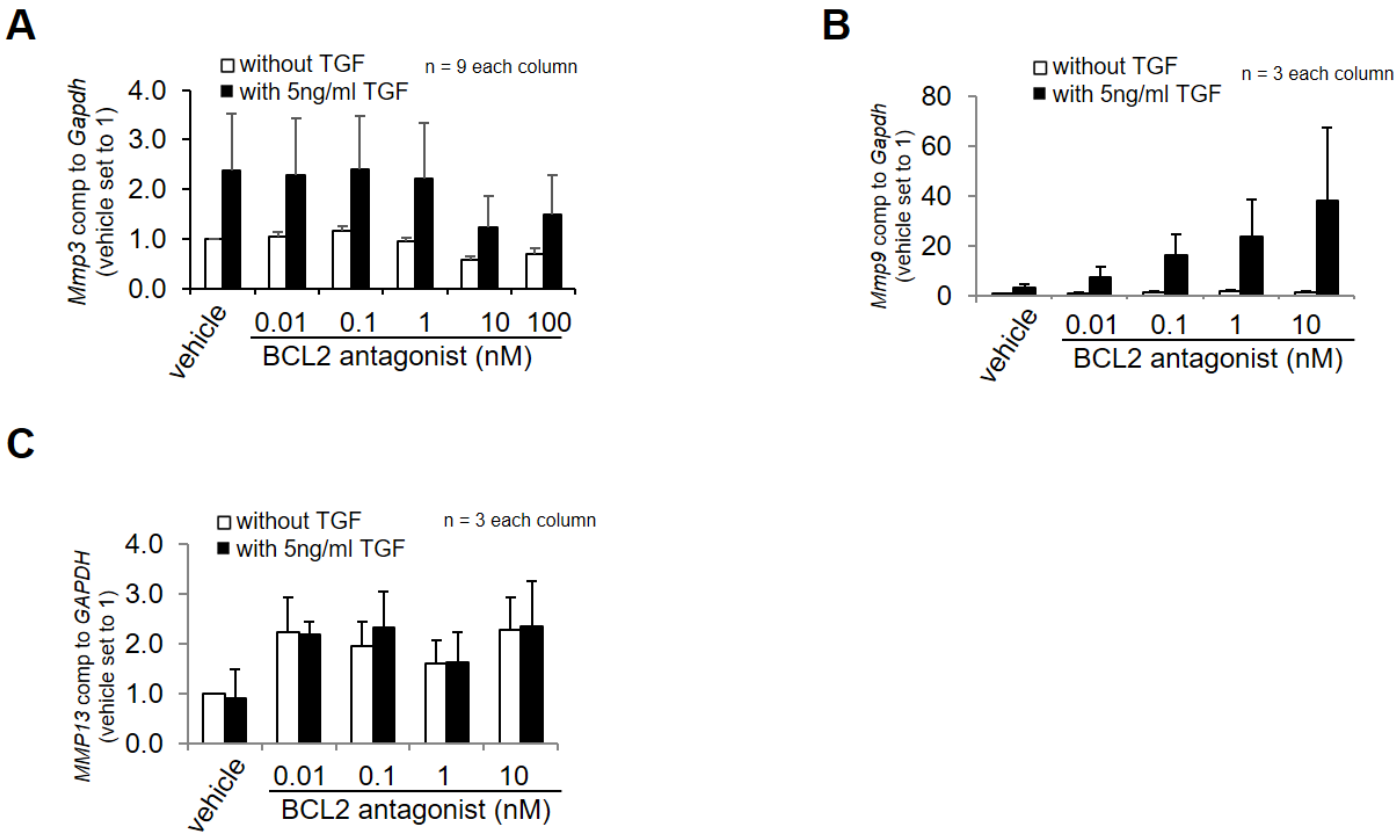

Supplementary figure 4: ***Mmp3*** **increased upon TGFβ stimulation and decreased following administration of high-dose BCL2 antagonist compared to vehicle.** ***Mmp9*** **increased dose-dependently following administration of BCL2 antagonist compared to vehicle.** ***Mmp13*** **did not change dose-dependently upon BCL2 antagonist regardless of TGFβ stimulation.** qPCR with murine fibroblasts stimulated with 5 ng/ml TGFβ, BCL2 antagonist stimulation for 24 h. (A) *Mmp3*. (B) *Mmp9*. (C) *Mmp13*. n as indicated, not significant, ANOVA, Dunn's multiple comparison test.

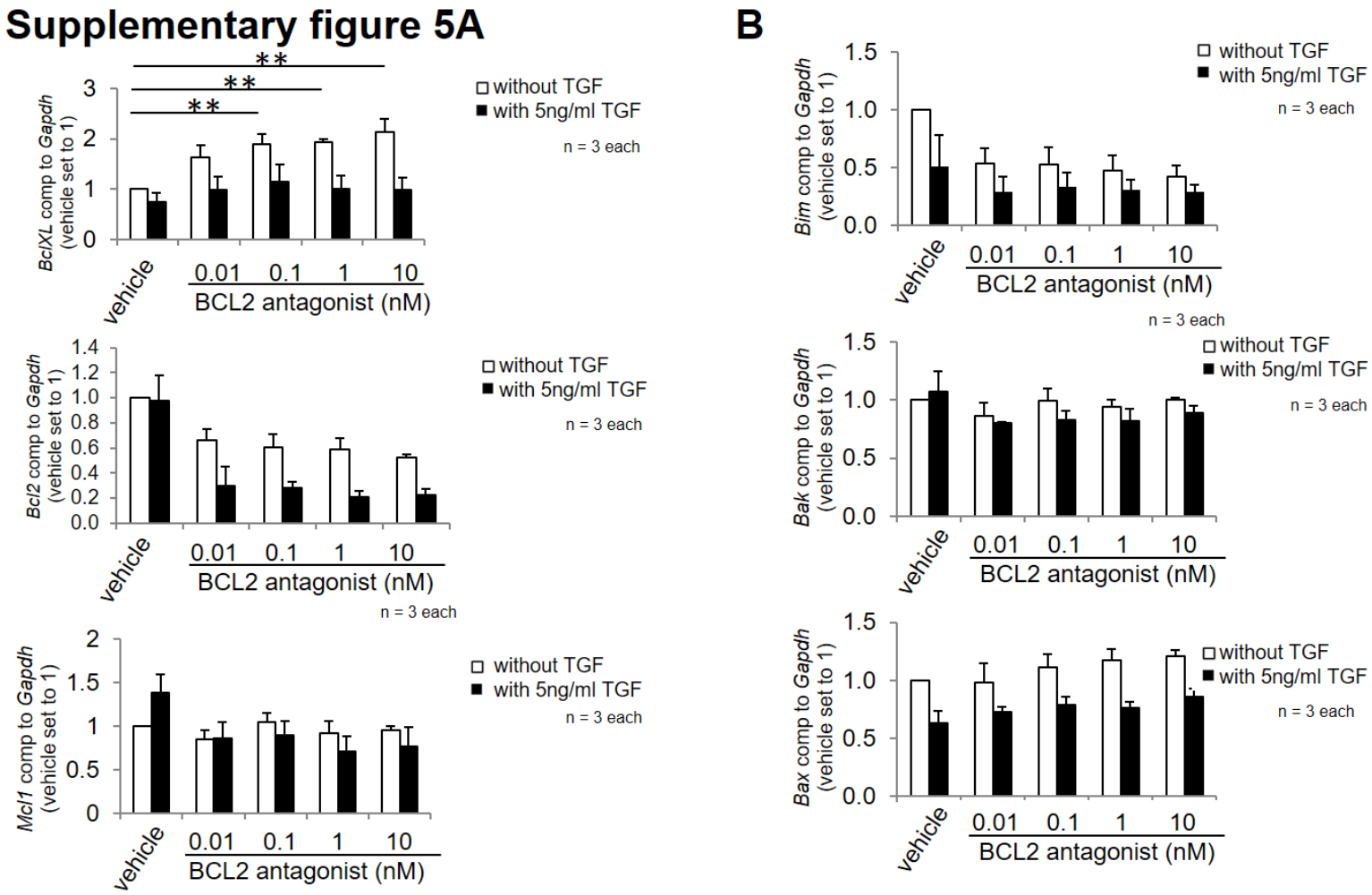

Supplementary figure 5: ***BclXL* dose-dependently increased following administration of BCL2 antagonist compared to vehicle. *Bcl2, Mcl1, Bim, Bak* and *Bax* were not changed.** qPCR with murine fibroblasts stimulated with 5 ng/ml TGFβ, BCL2 antagonist stimulation for 24 h. (A) Pro-survival *BclXL, Bcl2* and *Mcl1*. (B) Pro-apoptotic *Bim, Bak* and *Bax*. ** p < 0.01, ANOVA, Dunn's multiple comparison test.

Supplementary figure 6

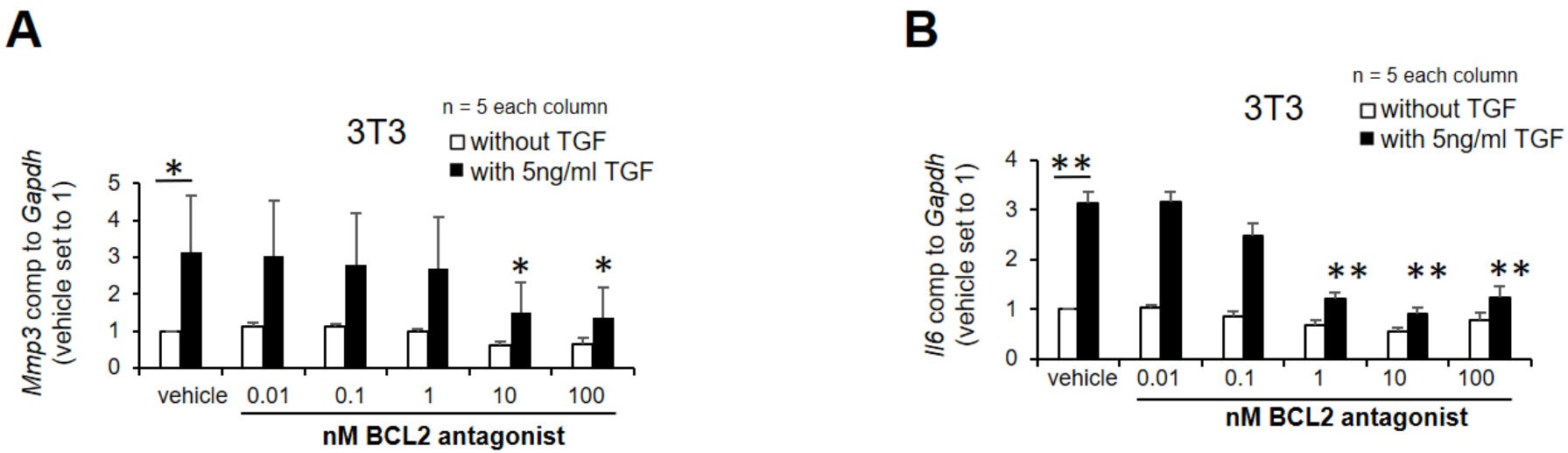

Supplementary figure 6: ***Mmp3* and *Il6* dose-dependently decreased in 3T3 fibroblasts following administration of the BCL2 antagonist compared to vehicle.** qPCR with murine fibroblasts 3T3 stimulated with 5 ng/ml TGFβ, BCL2 antagonist stimulation for 24 h. (A) *Mmp3*. (B) *Il6*. ANOVA, Dunn's multiple comparison test. Mean value und standard deviation are shown. * $p < 0.05$, ** $p < 0.01$.

Supplementary figure 7

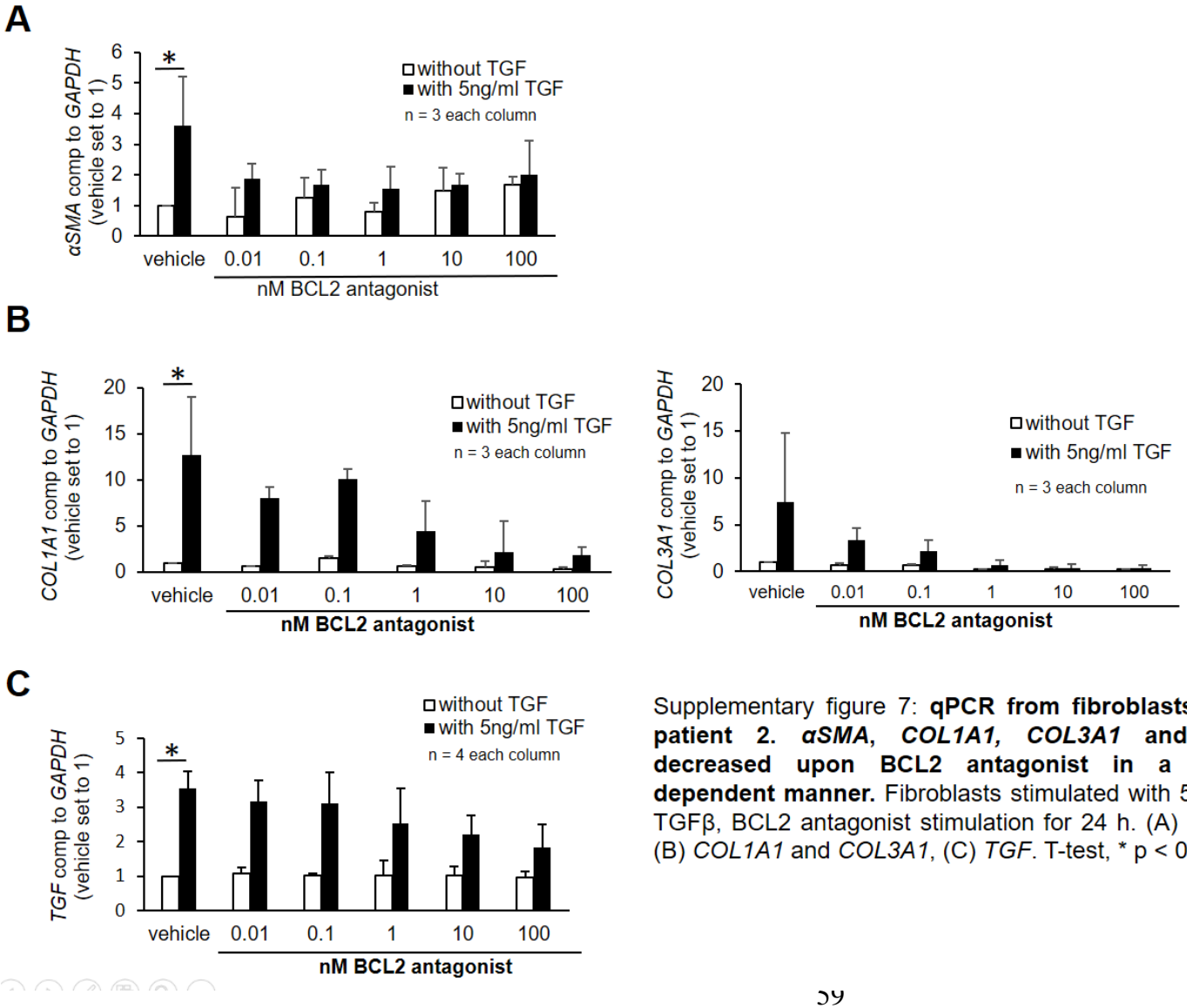

Supplementary figure 7: **qPCR from fibroblasts from patient 2. *αSMA*, *COL1A1*, *COL3A1* and *TGF* decreased upon BCL2 antagonist in a dose-dependent manner.** Fibroblasts stimulated with 5 ng/ml TGFβ, BCL2 antagonist stimulation for 24 h. (A) αSMA, (B) *COL1A1* and *COL3A1*, (C) *TGF*. T-test, * $p < 0.05$.

Supplementary figure 8

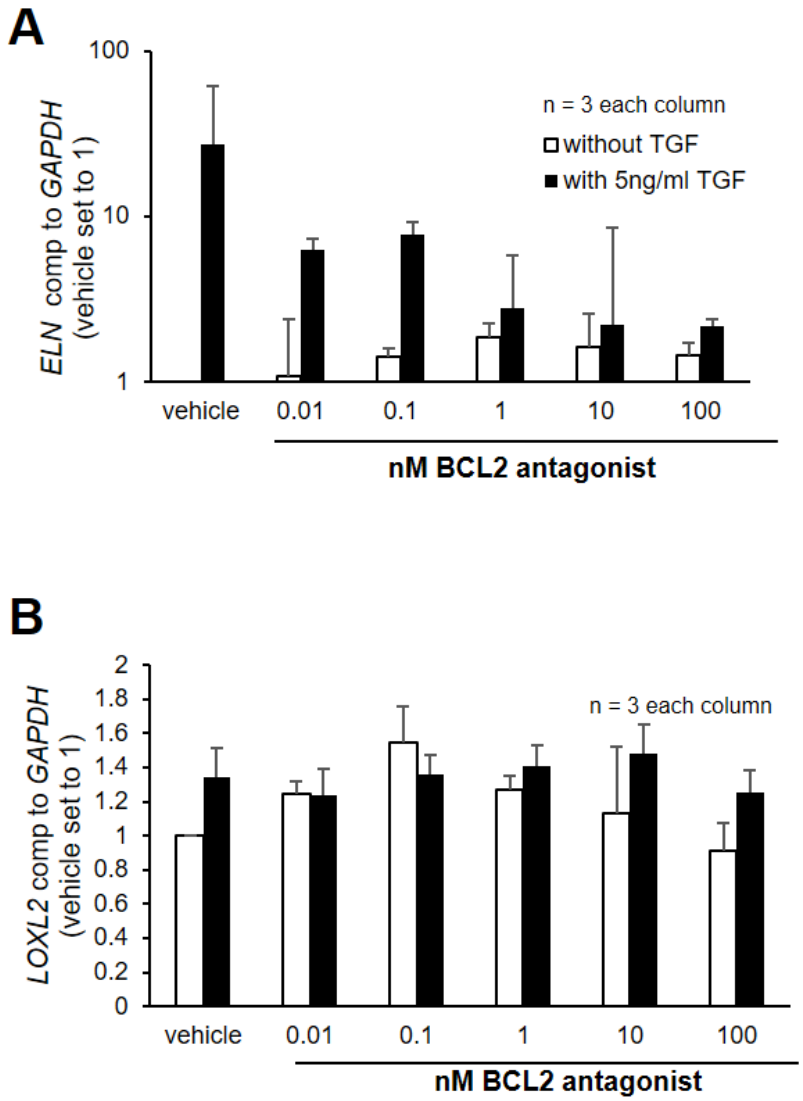

Supplementary figure 8: **qPCR from fibroblasts from patient 2. *ELN* decreased upon BCL2 antagonist in a dose-dependent manner.** Fibroblasts stimulated with 5 ng/ml TGFβ, BCL2 antagonist stimulation for 24 h. (A) *ELN*, (B) *LOXL2*. ANOVA, Dunn's multiple comparison test.

Supplementary figure 9A

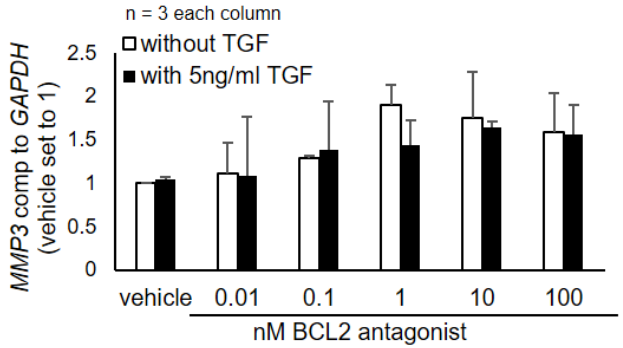

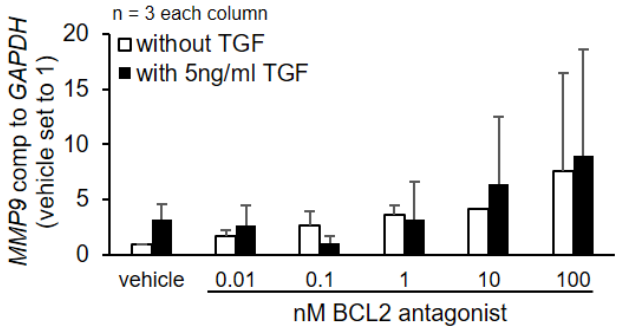

B

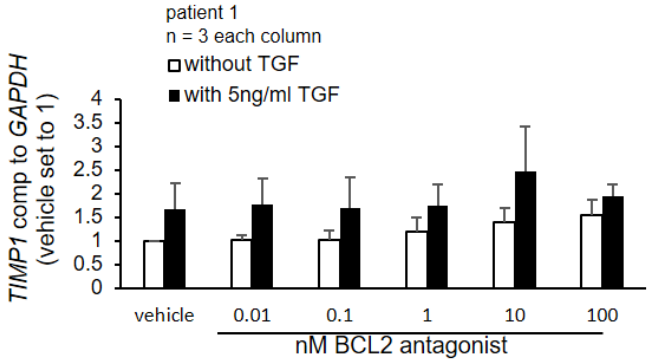

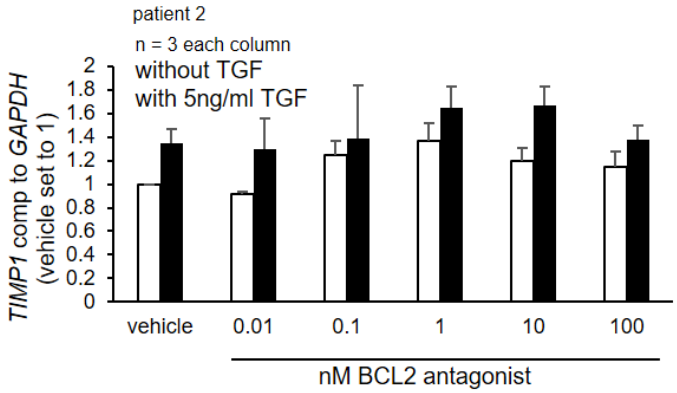

Supplementary figure 9: ***MMP3*, *MMP9* and *TIMP1* mRNA were unchanged following administration of BCL2 antagonist in fibroblasts from patient 1.** qPCR with fibroblasts stimulated with 5 ng/ml TGFβ, BCL2 antagonist stimulation for 24 h with the concentrations indicated. (A) *MMP3* and *MMP9*. (B) *TIMP1* for patient 1 (left) and 2 (right). ANOVA, Dunn's multiple comparison test.

Supplementary figure 10 A

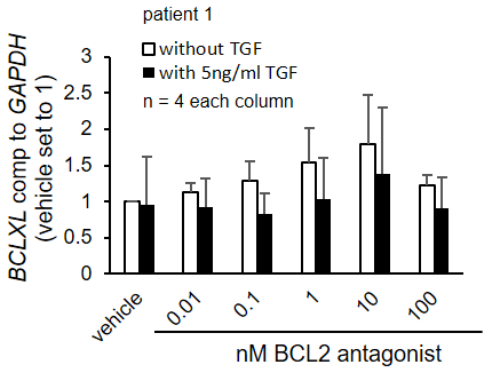

B

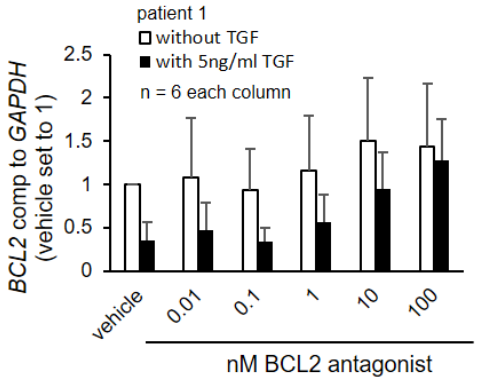

C

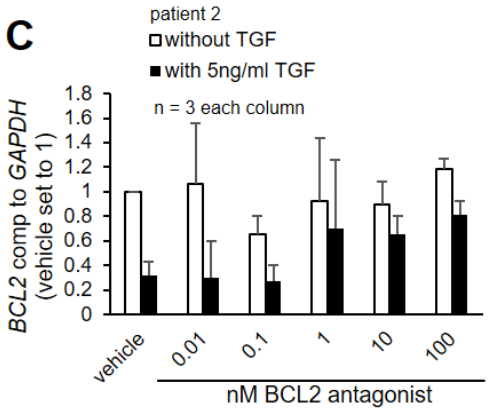

Supplementary figure 10: ***BCLXL* and *BCL2* mRNA remained unchanged following administration of BCL2 antagonist in human primary fibroblasts.** qPCR with fibroblasts stimulated with 5 ng/ml TGFβ, BCL2 antagonist stimulation for 24 h with the concentrations indicated. (A) *BCLXL* in fibroblasts from patient 1. (B) *BCL2* in fibroblasts from patient 1. (C) *BCL2* in fibroblasts from patient 2. ANOVA, Dunn's multiple comparison test.